Virulence

ISSN: 2150-5594 (Print) 2150-5608 (Online) Journal homepage: www.tandfonline.com/journals/kvir20

The *Pseudomonas aeruginosa sirB2* gene is a fitness determinant of anaerobic growth and its inactivation affects virulence and rugose small colony variants emergence

Valerio Baldelli, Stacy Julisa Carrasco Aliaga, Claudia Antonella Colque, Francesca Mazzola, Srikanth Ravishankar, Helle Krogh Johansen, Søren Molin, Nadia Raffaelli, Moira Paroni, Paolo Landini & Elio Rossi

To cite this article: Valerio Baldelli, Stacy Julisa Carrasco Aliaga, Claudia Antonella Colque, Francesca Mazzola, Srikanth Ravishankar, Helle Krogh Johansen, Søren Molin, Nadia Raffaelli, Moira Paroni, Paolo Landini & Elio Rossi (2026) The *Pseudomonas aeruginosa sirB2* gene is a fitness determinant of anaerobic growth and its inactivation affects virulence and rugose small colony variants emergence, Virulence, 17:1, 2605800, DOI: 10.1080/21505594.2025.2605800

To link to this article: https://doi.org/10.1080/21505594.2025.2605800

VIRULENCE
2026, VOL. 17, NO. 1, 2605800
https://doi.org/10.1080/21505594.2025.2605800

Taylor & Francis
Taylor & Francis Group

BACTERIAL PATHOGENESIS

OPEN ACCESS Check for updates

The *Pseudomonas aeruginosa sirB2* gene is a fitness determinant of anaerobic growth and its inactivation affects virulence and rugose small colony variants emergence

Valerio Baldelli [a*], Stacy Julisa Carrasco Aliaga [a*], Claudia Antonella Colque [b], Francesca Mazzola [c], Srikanth Ravishankar [a], Helle Krogh Johansen [b,d,e], Søren Molin [d], Nadia Raffaelli [f], Moira Paroni [a], Paolo Landini [a], and Elio Rossi [a]

[a]Department of Biosciences, University of Milan, Milan, Italy; [b]Department of Clinical Microbiology, Rigshospitalet, Copenhagen, Denmark; [c]Department of Clinical Sciences, Polytechnic University of Marche, Ancona, Italy; [d]Department of Clinical Medicine Faculty of Health and Medical Sciences, University of Copenhagen, Copenhagen, Denmark; [e]Novo Nordisk Foundation Center for Biosustainability, Technical University of Denmark, Denmark; [f]Department of Agricultural, Food and Environmental Sciences, Polytechnic University of Marche, Ancona, Italy

ABSTRACT

Pseudomonas aeruginosa is the leading cause of death in cystic fibrosis (CF) patients, yet the genetic mechanisms driving its fitness in the host remain poorly defined. Previously collected transcriptomic data of clinical samples showed that expression of the gene PA14_RS04555 (*sirB2*) is stimulated in the CF lung environment. In this work, we show that *sirB2* is regulated by the global transcriptional regulators Vfr and AmrZ. Loss of *sirB2* markedly enhanced *P. aeruginosa* pathogenicity, increasing virulence in *Galleria mellonella*, and promoting bacterial translocation and biofilm formation in a differentiated airway epithelial infection model. Deletion of *sirB2* triggered the emergence of biofilm-proficient rugose small colony variants (RSCVs), driven by elevated c-di-GMP and increased Pel polysaccharide production when cultures were grown in static conditions. The RSCV phenotype depends on suppressor mutations in the *wsp* operon, possibly as a response to redox imbalance caused by the lack of *sirB2* under oxygen-limited conditions. Indeed, the *sirB2* mutant exhibited impaired fitness during anaerobic respiration when nitrate was the sole electron acceptor, in a manner independent of the ubiquinone pool. Our findings show that *sirB2* inactivation promotes RSCV emergence and identify *sirB2* as a novel genetic determinant of metabolic fitness under host-relevant conditions, thereby underscoring the role of redox balance in chronic CF infections.

ARTICLE HISTORY
Received 26 June 2025
Revised 17 November 2025
Accepted 13 December 2025

KEYWORDS
Pseudomonas aeruginosa; rugose small colony variants; biofilm; virulence; anaerobic respiration; redox imbalance

Introduction

Pseudomonas aeruginosa is a common cause of acute and chronic infections in different human body niches, including the airways of cystic fibrosis (CF) patients [1,2]. Acute infections are characterized by the production of several virulence factors, such as toxins, proteases, type IV pili (T4P), and flagella, which are associated with substantial tissue damage and systemic spread and correlate with high mortality rates [3–6]. However, acute infections can often evolve into chronic ones, in which *P. aeruginosa* leads to unrelenting, non-productive inflammation, contributing to morbidity and mortality [2,3,7], despite showing minimal invasiveness and cytotoxicity due to reduced virulence factor production associated with switching from a planktonic lifestyle to biofilm communities [8].

Two second messengers orchestrate the phenotypic switch of *P. aeruginosa* during its transition from acute to chronic infections [9]. Cyclic AMP (cAMP) is synthesized by the two adenylate cyclases CyaA and CyaB, and, through its binding with the global regulator Vfr, activates expression of genes associated with acute virulence, such as proteases, elastase, and pyocyanin [9–11]. The activity of the cAMP-Vfr regulon is antagonized by the 3“,5”-cyclic diguanylic acid (c-di-GMP) second messenger. c-di-GMP intracellular concentrations are governed by the opposing actions of diguanylate cyclases (DGCs) and phosphodiesterases (PDEs), which either synthesize or degrade the molecule [12]. An increase in c-di-GMP concentrations is associated with phenotypes typical of chronic infections, promoting biofilm formation and arresting the production of acute virulence determinants [12]. For

CONTACT Elio Rossi elio.rossi@unimi.it; Paolo Landini paolo.landini@unimi.it
*Equally contributed to the work.
Supplemental data for this article can be accessed online at https://doi.org/10.1080/21505594.2025.2605800

example, high c-di-GMP levels trigger the production of the Pel polysaccharide, a polymer of partially de-*N*-acetylated 1,4-linked N-acetylgalactosamine, which constitutes a central element of the biofilm matrix and may play a direct role in pathogenesis by conferring protection against antibiotics and the host immune system [13,14].

Genome plasticity is a key factor underlining *P. aeruginosa* success as a pathogen. Accumulation of genetic mutations leads to the evolution of complex pathophenotypes that increase bacterial fitness within the host [15–17]. A typical example is the emergence of rugose small colony variants (RSCVs). RSCVs are slow-growing isolates characterized by a strong attachment to surfaces and auto-aggregation due to enhanced exopolysaccharide production [18,19]. RSCVs are one of the most prevalent phenotypes acquired by isolates from CF patients [19,20], and several studies have established a causal link with infection persistence in animal models [19,21]. RSCVs derive from genetic mutations in pathways controlling c-di-GMP biosynthesis [22–24], such as the Wsp or YfiBNR systems [19,25–27]. Although oxygen limitation, which in turn results in an imbalanced NADH/NAD^+ ratio, seems to contribute to the evolution of RSCVs [18,28,29], genetic drivers of increased RSCVs selection during long-term infection are still unknown. Similarly, recent *in vivo* gene expression studies have identified a specific transcriptional program of the pathogen in the host [30–32], where up to 60% of the identified genes are poorly characterized. Overall, this indicates a substantial lack of knowledge in *P. aeruginosa* biology during human infection and that molecular determinants of this bacterium's success in chronic infections are yet to be discovered [33].

In this work, we evaluate the role of the unknown function gene PA14_RS04555 (*sirB2*), identified by analyzing gene expression data from clinical isolates adapted to chronic infections in CF patients [32]. We show that *sirB2* expression is regulated by Vfr and AmrZ two *P. aeruginosa* key regulators involved in the adaptation to the host. Deletion of *sirB2* contributes to a loss in fitness during anaerobiosis and redox imbalance when oxygen availability is limited, increasing the frequency of RSCVs in the bacterial population, promoting biofilm formation, enhancing virulence factor production, and resulting in a hypervirulent phenotype.

Our results identify a novel genetic determinant whose disruption affects *P. aeruginosa* physiology in oxygen-limited conditions, favoring the switch to the RSCVs phenotype. Overall, this shows that mining *in vivo* gene expression datasets and functional characterization based on classic genetic approaches are essential for advancing our understanding of the molecular determinants underlying *P. aeruginosa* pathogenicity and survival within the host.

Materials and methods

Bacterial strains, plasmids, and growth conditions

The bacterial strains and plasmids used in this study are listed in Supplementary Table S1 (Table S1). Mutants were generated using homologous recombination, as previously described [34,35], with minor modifications. Suicide vectors were obtained using the USER cloning technique, designing cloning primers with the AMUSER software [36]. All primers used in this study are listed in Supplementary Table S2 (Table S2). Strains were routinely grown in Lysogeny Broth (LB) medium (tryptone 10 g/l, yeast extract 5 g/l, NaCl 5 g/l) at 37°C with shaking (200 rpm) unless otherwise stated or in SCFM2 medium [37]. Antibiotics were added at the following concentrations: gentamicin, 100 µg/ml for *P. aeruginosa* and 20 µg/ml for *E. coli*; tetracycline 100 µg/mL for *P. aeruginosa* and 20 µg/ml for *E. coli*; carbenicillin, 400 µg/ml for *P. aeruginosa* and 100 µg/ml for *E. coli*; chloramphenicol, 30 µg/ml for *E. coli*.

P. aeruginosa growth in anaerobiosis was performed in 96-well microtiter plates in LB or M9 minimal medium (42 mM Na_2HPO_4, 22 mM KH_2PO_4, 8.5 mM NaCl, 19 mM NH_4Cl, 0.2 mM $CaCl_2$, 1 mM $MgSO_4$), using as electron acceptors either 100 mM KNO_3 or 40 mM arginine (LB arg) as specified. For growth in minimal medium 20 mM glucose (M9G), 20 mM sodium succinate, or 20 mM sodium succinate and citrate as carbon source (M9S/C) were used as carbon sources. Microtier plates were then incubated in anaerobic jars using AnaeroGen™ sachets (Thermo Scientific, 10,269,582). For ubiquinone experiments, a stock solution of UQ_9 (MedChemExpress, HY-101415) was prepared in ethanol (EtOH) at a concentration of 10 mM and used at a final concentration of 5 µM. Samples grown in the presence of the solvent vehicle EtOH [0.05% (v/v)] were used as controls in each microtiter plate.

The strains used in ALI infections were tagged with the sGFP fluorophore (Excitation: 488 nm/Emission: 510 nm), following the protocol described by Choi and colleagues [38] using four-parental conjugation, with the mini-Tn7 delivery plasmid pJM220.

Promoter analysis and measurements of promoter activity

A ~400 bp sequence upstream of the *sirB2* gene starting codon was selected as the possible promoter region.

Then, promoter analysis was performed using the BPROM (www.softberry.com), SAPPHIRE [39], and PRODORIC [40] online software.

Bioluminescence was determined as a function of population density by using an EnSight Multimode plate reader (PerkinElmer), as previously described [41]. Briefly, overnight cultures of the *P. aeruginosa* PA14 reporter strains used in this study (Table S1) harboring the *sirB2* or *cdrA* promoter region transcriptionally fused with the *luxCDABE* operon (P*sirB2::luxCDABE*, P*cdrA::luxCDABE*) were diluted in 200 µL of LB to an OD_{600} ≈0.1, or an OD_{600} ≈0.02, respectively, and dispensed into 96-well black clear-bottom microtiter plates. For P*sirB2* promoter, the strains were grown either in LB or in SCFM2 and luminescence and turbidity were determined every 2 h of incubation at 37°C with gentle shaking (120 rpm) or in static conditions for 24 h. For the P*cdrA* promoter, luminescence and turbidity were determined after 20 h at 37°C in static conditions. Reporter activity was determined as RLU/OD_{600} for each sample.

Galleria mellonella *killing assay*

The *G. mellonella* killing assay was performed as previously described [42,43]. Briefly, *G. mellonella* caterpillars in the final instar larval stage (average weight, 500 mg) were infected with 10 µL of saline containing about five bacterial cells of each *P. aeruginosa* PA14 strain (WT and mutant) used in this work. *G. mellonella* larvae were incubated at 37°C in petri dishes (10 larvae per dish) and monitored for 72 h. Larvae were considered dead when they did not respond to gentle prodding. At least 30 larvae per condition were used in four independent experiments. Survival curves for the *G. mellonella* killing assay were generated using the Kaplan–Meier method.

Cell cultures

Cell cultures were established essentially as previously described [44]. In particular, BCi-NS1.1 cells were seeded in Pneumacult™-Ex Plus Medium (StemCell, 05040) and passaged at least two times before plating 1.5×10^5 cells onto 6.5-diameter-size transwells with 0.33 cm^2/0.4 µm pore polyester membrane inserts (Corning Incorporated, 3470), previously coated with human type I collagen (Gibco, A1048301). Cultures were maintained under submerged conditions until fully confluent. On days 3–4, cells were air-lifted, and the basolateral chamber medium was replaced with Pneumacult-ALI maintenance medium (STEMCELL Technologies, 05001). Pneumacult-ALI maintenance medium was supplemented with Pneumacult-ALI 10x supplement (STEMCELL Technologies, 05003), Pneumacult-ALI maintenance supplement (STEMCELL Technologies, 05006), 480 ng/mL hydrocortisone, and 4 µg/mL heparin (STEMCELL Technologies, 07980). ALI cultures were grown in a 37°C, 5% CO_2 humidified incubator for 30 days, with media replacement every 2–3 days. Epithelial polarization was monitored by measuring transepithelial electrical resistance (TEER) with a chopstick electrode (STX2; World Precision Instruments). After 15 days under ALI conditions, the apical surface was washed with 1x Phosphate Buffered Saline (PBS) every 3–4 days to remove accumulated mucus.

Bacterial infections of ali cultures

Bacterial infections of ALI cultures were performed as previously described [44]. Fluorescently labeled bacterial strains were grown overnight in LB at 37°C in shaking conditions (180 rpm). The cultures were diluted to an OD_{600} of 0.05, grown in LB to the exponential phase (OD_{600} = 0.4–0.6), washed, and resuspended in PBS at a density of 10^5 CFU/mL. ALI cultures, prepared as described above, were inoculated with 10^3 CFU on the apical side diluted in 10 µL PBS, and co-cultures were grown for 14 h in a 37°C, 5% CO_2 humidified incubator. Control wells were incubated with PBS free of bacteria. The initial inoculum was confirmed by plating serial dilutions on an LB-agar plate and counting the colonies. Following infection, 200 µL of PBS was added to the apical side, and the TEER was measured. The apical solution and the basolateral medium were collected to quantify CFU on both chambers of the transwells by plating 10 µL of sixfold serial dilutions on LB-agar plates in technical replicates. Additionally, attached bacteria to the ALI cultures were counted by adding 200 µL of 0.1% Triton to the wells and scraping the filter. The basolateral media were also collected to measure LDH release and determine induced epithelial cytotoxicity. LDH release was quantified using the Invitrogen™ CyQUANT™ LDH Cytotoxicity Assay Kit (Invitrogen, C20301) according to the manufacturer´s instructions by using 50 µL of basolateral media per sample in triplicate. The absorbance was measured at 680 nm and 490 nm.

For confocal microscope analysis and visualization, ALI cultures on transwell inserts were rinsed once with PBS and fixed by adding 4% (wt/vol) paraformaldehyde (PFA) to both apical and basolateral chambers for 20 min at 4°C. After washing, cells were permeabilized and blocked for 1 h with a buffer containing 3% Bovine Serum Albumin (BSA), 1% Saponin, and 1% Triton X-100 in PBS. Cells were stained on the apical side

with Phalloidin-AF555 (Invitrogen, A34055) and TO-PRO3 (Biolegend, 304,008) diluted in a staining buffer (3% BSA and 1% Saponin in PBS) at a 1:500 dilution for 2 h at room temperature. Transwells were removed from their supports with a scalpel and mounted on glass slides with VECTASHIELD® Antifade Mounting Medium (VWR, VECTH-1000). Images were acquired with a Stellaris 8 confocal laser scanning microscopy (63x magnification, 1.3 oil) and analyzed using the ImageJ software.

Biofilm and pellicle formation assay

The crystal violet binding assay was performed in microtiter plates as previously described [45–47]. Bacterial cells were grown in LB broth or in SCFM2 for 16 h in shaking conditions and diluted to OD_{600} ≈0.02 in the same medium. Aliquots of 200 µl were transferred to a sterile 96-well polystyrene microtiter plate and incubated at 37°C for 24 h in static conditions. The liquid phase was removed, and the attached cells were stained with 0.1% (w/v) crystal violet (Sigma-Aldrich, C6158) for 15 min. After washing the wells four times with distilled water, the surface-associated dye was solubilized with 200 µL of ethanol. The A_{595} of the dye solutions was measured in the automated EnSight Multimode plate reader (PerkinElmer).

To visualize pellicle formation, bacterial cultures were grown for 16 h at 37°C with shaking in LB broth. Then, cultures were diluted in 10 mL of fresh medium to reach an OD_{600} ≈0.015 in 50 mL tubes and incubated at 37°C in static conditions [48]. The OD_{600} was measured after 24 h. Cultures were centrifuged, and the cell pellets were resuspended in 40 µg/mL Congo-Red and incubated for 2 h at 37°C with gentle shaking (120 rpm). After centrifugation, the A_{490} of cell-free supernatants were measured and normalized to the cell density of bacterial cultures.

Phenotypic assays

Pyocyanin, pyoverdine, proteases, and elastase were measured in cell-free culture supernatants of *P. aeruginosa* PA14 strains as previously described with minor modification [49,50]. Briefly, *P. aeruginosa* PA14 overnight cultures were diluted to an OD_{600} of ≈0.02 in LB broth, and 200 µL were dispensed in 96-well microtiter plates. The plates were incubated at 37°C in static conditions for 24 h. After incubation, eight independent cultures of the same strain were pooled, the OD_{600} was measured, and cell-free supernatants were collected into 2 mL tubes for pyocyanin, pyoverdine, elastase, and protease quantification.

For pyocyanin, after extraction with an isovolume of chloroform, the pyocyanin-containing chloroform phase was transferred into clean 2 mL tubes and acidified with an isovolume of 0.2 N HCl. After centrifugation, 900 µL of the aqueous phase were transferred into 96-well microtiter plates, and the amount of extracted pyocyanin was measured at an absorbance of 520 nm (A_{520}).

For pyoverdine, 100 µL of the cell-free supernatants were appropriately diluted in 100 mM Tris-HCl (pH 8.0) and measured as the A_{405} normalized to the cell density of bacterial cultures.

For both elastase and protease activity, 40 µL of cell-free supernatants were added to 1.5 mL tubes containing the elastin-Congo red (Sigma-Aldrich, E0502) reaction buffer and the azocasein (Sigma-Aldrich, A2765) reaction buffer, respectively. Finally, the elastolytic and proteolytic activity were measured at A_{495} and A_{400}, respectively, using the EnSight Multimode plate reader (PerkinElmer).

Rugose Small Colony Variants (RSCVs) were isolated onto Congo Red Agar plates containing 10 g/L tryptone (Oxoid, LP0042B), 10 g/L Bacto agar (BD, 214,010), 40 µg/ml Congo Red (Sigma-Aldrich, C6767) and 15 µg/mL brilliant blue R (Sigma-Aldrich, B7920). *P. aeruginosa* PA14 overnight cultures were diluted to an OD_{600} of ≈0.02 in LB or in SCFM2 and 200 µL were dispensed in 96-well microtiter plates. The plates were incubated at 37°C in static conditions for 24 h. After incubation, serial 1:10 dilutions were made for each well until 10^{-9}. 100 µL of the proper dilution was then plated onto CR agar plates for colony counting and visualization. For each plate, the percentage of RSCVs was calculated as the number of the RSCVs (red) divided by the total number of colonies.

For the colony biofilm assay, 3 µL of overnight PA14 cultures was spotted onto CR agar plates. Biofilms were grown at 25°C for at least 72 h before images were acquired.

Whole-genome, targeted DNA sequencing and genomics analysis

The Genomic DNA was extracted using the GenElute Bacterial Genomic Kit (Merck, NA2110) from *P. aeruginosa* overnight cultures of selected strains. Library preparation was performed by Eurofins Genomics Europe and sequenced using an Illumina NovaSeq machine with an approximate coverage of > 150-fold. Reads were trimmed, and low-quality reads and potential contamination from adapters were removed using Trimmomatic (v 0.35) tool. Using the BWA MEM algorithm, high-quality sequences were aligned against the *P. aeruginosa* PA14 genome (NC_008463.1). Reads

coverage was calculated using the bamCoverage tool with a bin size of 50 bp, and large deletions were identified from the bedgraph files as areas with zero coverage. Deletions were visually confirmed by inspecting the aligned reads in the Integrative Genomics Viewer (v 2.16.2). In all the *P. aeruginosa* laboratory strains tested and in the single RSCVs, the 318bp-long deletion in the *wspC* and *wspD* genetic locus (from nt 1,408,822 to nt 1,409,140 of the PA14 genome) was verified via PCR by the amplification with the primers couple Fw_*wspCseq* (GTCTTTCGTGTTCCGCCGGAC CA) and Rv_*wspDseq* (AATGGATAGGATTCATCGG CGCCACTTC) and then sequenced by Sanger sequencing through Eurofins Genomics Europe.

For the evaluation of *sirB2* sequence conservation in clinical isolates raw reads from Marvig et al. [16], Núñez-García et al. [51] and Spilker and LiPuma [52] were obtained from the Sequence Read Archive (SRA). Raw reads were mapped against either *P. aeruginosa* PAO1 (NC_002516.2) or *P. aeruginosa* UCBPP-PA14 (NC_008463) genomes using BWA MEM (v0.7.17) with default parameters. Variant calling was performed on the *sirB2* gene region (PAO1: 4,545,389– 4,545,745/ positive strand; UCBPP-PA14: 980,731 – 981,087/negative strand) using "bcftools mpileup" and "bcftools call." SNPs and INDELs were filtered based on quality (QUAL ≥60 for SNPs, ≥ 500 for INDELs), mapping quality (MQ ≥ 25), and read depth (DP > 15 for SNPs, > 20 for INDELs). Filtered variants were applied to the reference to reconstruct sample-specific consensus sequences using "bcftools consensus." Consensus nucleotide sequences were translated using EMBOSS "transeq." Sequences were aligned with "MAFFT – auto," and codon-aware alignments were generated using PAL2NAL. Approximately maximum-likelihood phylogenetic trees were inferred with FastTree based on the codon alignments. The generated codon alignment and inferred tree were used to evaluate the selection pressure on the *sirB2* gene using the FUBAR method implemented in HyPhy package. Conservation analysis was performed on the codon alignment by computing pairwise sequence identity, counting variable codon positions, and estimating the global dN/dS ratio based on synonymous and nonsynonymous substitutions using the standard genetic code, using the custom Python script "sirb2_conservation_analysis.py."

Determination of intracellular NAD$^+$ and NADH

All chemical reagents were obtained from Merck. NAD and NADH extraction were performed according to the NAD/NADH-Glo™ assay protocol (Promega, G9071) with minor modifications. A cellular pellet, derived from 1.6×10^8 CFU, was resuspended in 160 µl of phosphate-buffered saline, and cells were lysed by adding 160 µl of a solution containing 0.2 N NaOH and 1% dodecyltrimethylammonium bromide (DTAB). Lysed cells were divided into two 150 µl-aliquots. One aliquot was incubated at 60°C for 20 min for NADH extraction. The other aliquot was mixed with 75 µl of 0.4 N HCl prior incubation at 60°C for 20 min for NAD extraction. After 10 min at room temperature, both samples were centrifuged at 20.000 x *g* for 5 min and supernatants were neutralized with 150 µl of 0.2 N HCl/0.25 M Trizma base solution (for NADH extraction) or 75 µl of 0.5 M Trizma base (for NAD extraction). Neutralized samples were used to quantify NAD and NADH using a well-established fluorometric cycling assay [53,54] with minor modifications. Briefly, appropriate volumes of samples were spiked with known amounts of NAD or NADH (ranging from 0.1 to 2 pmol) in a final volume of 100 µl of water, in the wells of a 96-well microplate. The fluorometric reaction was initiated by adding 100 µl of the cycling reagent to each well. The cycling reagent was composed of 100 mM Tris-HCl, pH 8.0, 2% ethanol, 30 µM resazurin, 10 U/mL alcohol dehydrogenase, 0.1 mg/mL bovine serum albumin, 10 µM flavin mononucleotide and 0.1 mg/mL diaphorase. Diaphorase was previously purified through a PD MiniTrap Sephadex G-25 column (GE Healthcare) equilibrated and eluted with 10 mM Tris-HCl buffer, pH 8.0. The increase in resorufin fluorescence was continuously monitored at 32°C in a Synergy HT microplate reader (Bio-Tek, Winooski, VT, USA) equipped with 530 and 590 nm excitation and emission filters, respectively. The rates of fluorescence increase in individual wells were recorded and plotted against the respective nucleotide concentration. The nucleotide concentration in the sample was calculated from the slope/intercept ratio of the spike standard curve, considering the dilution factor.

Results

The sirB2 domain-containing gene PA14_RS04555 encodes an inner membrane protein conserved in Pseudomonas aeruginosa and belongs to the Vfr and AmrZ regulons

Expression of the PA14_RS04555 (*sirB2* hereafter) gene was previously found to be stimulated in *P. aeruginosa* clinical isolates growing in the lungs of chronically infected CF patients compared to standard laboratory conditions [32]. *sirB2* codes for a small inner membrane protein with four transmembrane passages. The gene is localized between the *oprG* gene and an uncharacterized operon coding for a putative epimerase

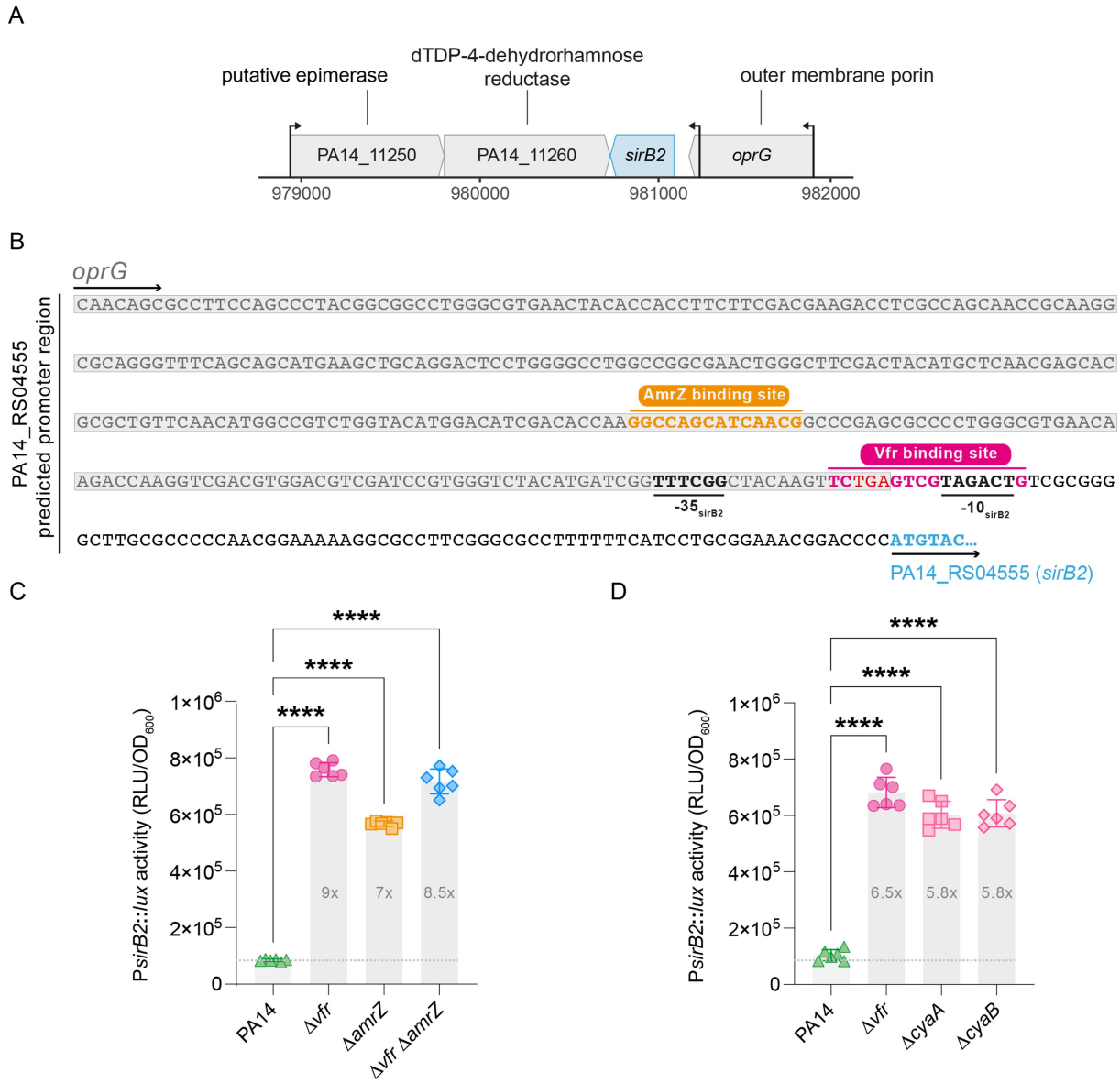

Figure 1. Expression, conservation, and regulation of the PA14_RS04555 (*sirB2*) gene in *P. aeruginosa* PA14. (A) The *sirB2* genetic locus in the genome of *P. aeruginosa* UCBPP-PA14 strain. (B) Schematic representation of the predicted *sirB2* promoter region. Position of the *oprG* gene, the AmrZ binding site, the −35 and −10 boxes, the Vfr binding site, and the *sirB2* gene ATG codon are reported. (C) Activity of the P*sirB2* promoter, reported as RLU/OD_{600}, in PA14, Δ*vfr*, Δ*amrZ* and Δ*vfr*/Δ*amrZ* knockout mutants. Cultures were grown at 37°C under shaking conditions for 8 h. Results from six independent experiments are reported with sd. ****, $p < 0.0001$ (ANOVA and Tukey's hypothesis test for multiple comparisons). (D) Activity of the P*sirB2* promoter, reported as RLU/OD_{600}, in PA14, Δ*vfr*, Δ*cyaA*, and Δ*cyaB* knockout mutants cultures grown at 37°C under shaking conditions for 8 h. Six independent experiments are reported with sd. ****, $p < 0.0001$ (ANOVA and Tukey's hypothesis test for multiple comparisons).

(PA14_11260) and a protein belonging to the dTDP-4-dehydrorhamnose reductase family (PA14_11250) (Figure 1A). We named the gene *sirB2* gene (UniProt id: A0A9Q9K1N2) as its product shares homology with SirB2 of *Salmonella enterica* serovar Typhimurium (BLASTP: identity 35.9%; coverage 92%), which is involved in pathogenicity and invasion [55,56].

The analysis of the *sirB2* locus in the genome sequences of 577 clinical isolates from CF patients in three independent cross-sectional studies [16,51,52] spanning ca. 10 years of adaptation detected minimal genetic variation within the *sirB2* coding region, regardless of the use of *P. aeruginosa* PAO1 or PA14 genomes as reference. Although the number of isolates with detectable mutations varied depending on the reference used (Fig. S1A), only 27 distinct nucleotide variants were observed, of which 10 were nonsynonymous (Fig. S1 and Data S1 [57]). No insertions,

deletions, or frameshifts were identified; instead, only missense variants were present at low frequency and targeted all predicted topological domains (Fig. S1B). Codon-based alignments confirmed the high conservation of *sirB2*, with mean pairwise identities of 98.91% (PAO1-based) and 98.79% (PA14-based), and only 26 out of 118 codons showing variability in either dataset. Approximate global dN/dS values derived from sequence-wide substitution counts were low (0.727 for PAO1; 0.720 for PA14), indicative of purifying selection. HyPhy analyses under full codon models further indicate the presence of strong evolutionary constraints, as calculated global ω estimates were well below 1 (PA14 = 0.0587; PAO1 = 0.0794), suggesting that SirB2 function is maintained during adaptation to CF airways.

At first, we searched for specific cues that could drive *sirB2* expression *in vivo*, focusing on the nutritional environment and oxygen availability, two of the significant differences between *in vivo* and *in vitro* conditions [32].

Thus, we cloned a ~ 400 bp sequence upstream of the *sirB2* gene into a mini-CTX:*lux* promoter probe and compared its activity in the wild-type strain PA14 (PA14 P*sirB2*:*lux*) during a 24-h growth between LB and SCFM2, *i.e.*, a medium mimicking the nutritional conditions in CF airways [37], both in shaking and static conditions (Fig. S2). No major differences could be observed at the level of strain growth (Fig. S2A). Promoter activity was maximal during the late exponential phase (ca. 8 hours) in all tested conditions and declined in the stationary phase, particularly in static cultures (Fig. S2B and S2C). We observed negligible, albeit statistically significant, differences between static and shaking growth during the late exponential phase (Fig S2B and S2C, max. 1.6 SCFM2/static vs SCFM2/shaking at 6/8 hours) in both media, while a 3-time reduction in the expression in static conditions was observed at 24 h of growth in LB medium (3-times higher in shaking). Thus, gene expression kinetics were affected by oxygen availability, while no significant differences were observed comparing LB and SCFM media. Therefore, LB medium was used for all subsequent experiments.

We then searched for transcriptional regulators that could drive the *sirB2* expression. Using the BPROM, SAPPHIRE, and PRODORIC tools, we analyzed the 400 bp-long sequence we used in the promoter activity assay, identifying potential −35 (5'-TTTCGG-3') and −10 (5'-TAGACT-3') promoter sequences and the putative binding sites for the AmrZ and Vfr transcriptional factors (Figure 1B), both involved in the regulation of infection-related processes and adaptation to the host [10,58–60]. The two sequences shared a high degree of similarity with the regulators' consensus sequences. While the predicted AmrZ box was located upstream of the main promoter elements, the Vfr box overlapped with the predicted *sirB*2 -10 region, a characteristic observed in promoters where Vfr acts as a repressor [58].

To verify the *in silico* predictions, we used the same mini-CTX:*lux* fusion to compare the *sirB2* promoter activity in the wild-type strain with that measured in Δ*amrZ*, Δ*vfr*, and Δ*amrZ*Δ*vfr* isogenic mutants.

Inactivation of either AmrZ or Vfr induced a seven- to eight-fold induction in the reporter activity (Figure 1C), indicating that both transcriptional regulators could act as repressors. The promoter activity in the Δ*vfr*Δ*amrZ* mutant was similar to either single mutant, suggesting that negative regulation by Vfr and AmrZ is not additive.

Since Vfr activity depends on cAMP levels for most genes, we measured luciferase activity in a genetic background lacking either one of the two adenylate cyclases (Figure 1D). As for the inactivation of the *vfr* gene, deletion of either the *cyaA* or *cyaB* genes led to a substantial increase in *sirB2* promoter activity, indicating that the Vfr repression of *sirB2* gene expression requires cAMP production.

Inactivation of the sirB2 gene enhances the pathogenic potential of P. aeruginosa PA14

Since *sirB2* is conserved in CF isolates and virulence-related regulators repress its expression, we hypothesized that the activity of the SirB2 protein might be involved in modulating virulence in the host. Therefore, we investigated the consequences of its absence, creating an isogenic deletion mutant in the standard laboratory strain PA14 and testing the strain in two different infection models.

At first, we monitored overall virulence using the *Galleria mellonella* larvae, an extensively used acute-infection model [42,61]. Assuming an average weight of a larva of ca. 500 mg, 10 µl of saline was used to inject each larva as a control vehicle without affecting the survival of the caterpillars (Figure 2A). Then, *G. mellonella* larvae were infected with approximately five cells of *P. aeruginosa* PA14 or the isogenic Δ*sirB2* mutant strain and incubated at 37°C for 48 h. Inactivation of the *sirB2* gene resulted in a significant increase in *P. aeruginosa* lethality. Only 2.5% of the larvae infected with the Δ*sirB2* strain survived at 12 h, compared to 92.5% of the wild-type strain at the same time point (Figure 2A). Since the mutation of the *sirB2* gene does not affect bacterial growth (Figure 2B), the

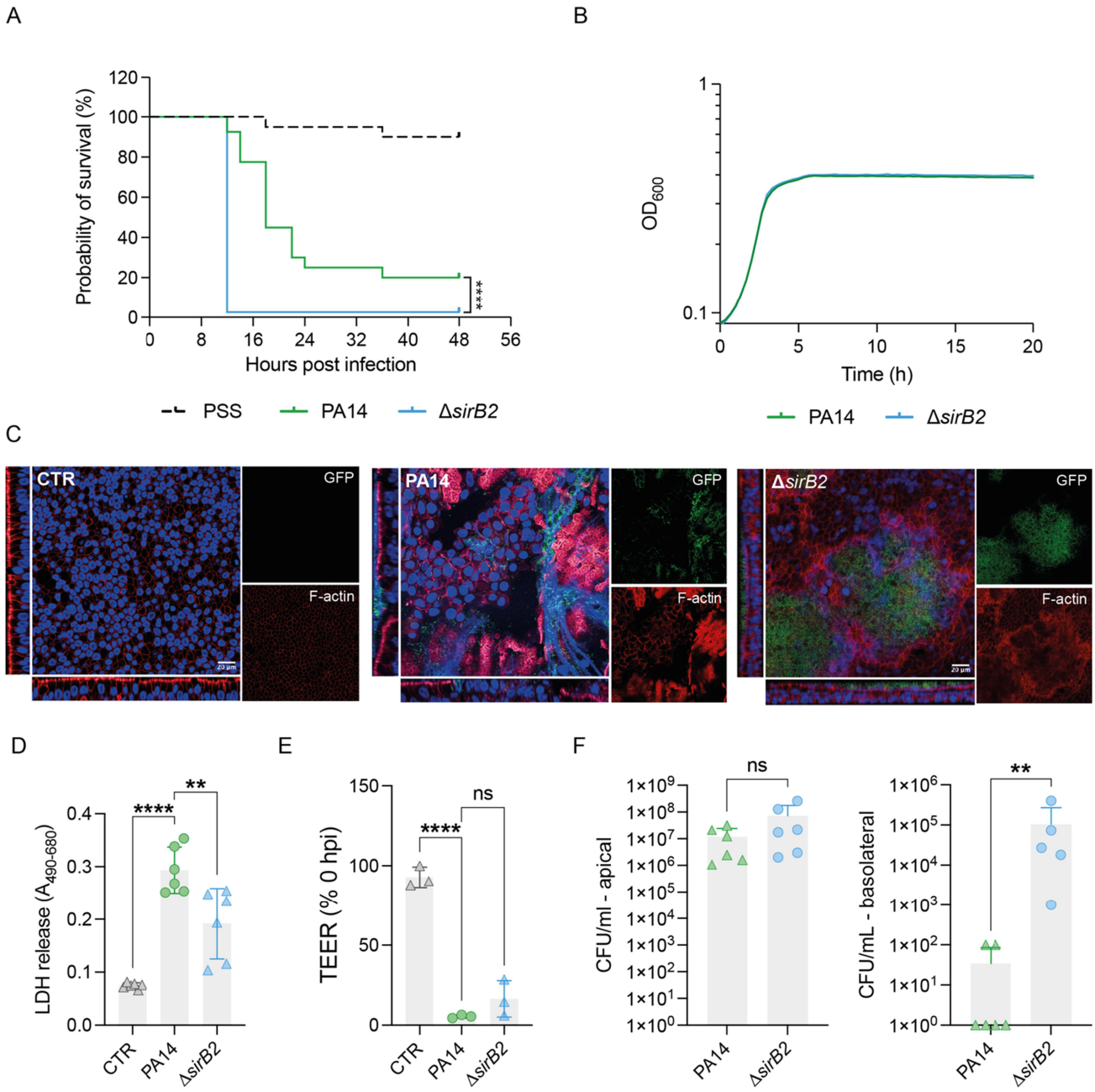

Figure 2. Effect of the *sirB2* gene deletion on *P. aeruginosa* PA14 pathogenicity in *in vivo* infection models. (A) Kaplan-Meier plot showing the percentage survival of *G. mellonella* larvae inoculated with *P. aeruginosa* PA14 and Δ*sirB2* strains. The mean survival rate calculated from four independent experiments performed on at least 50 larvae per condition is reported. ****, $p < 0.0001$ for PA14 vs. Δ*sirB2* (long-rank Mantel-Cox test). (B) Growth curves of PA14 and Δ*sirB2* incubated at 37°C in shaking conditions in lb medium. The average of at least three independent experiments is reported. (C) Confocal microscope imaging of epithelial ALI cell cultures on transwell incubated with PBS free of bacteria (CTR) or infected with PA14 or Δ*sirB2* strains constitutively expressing sGFP (green). One representative image from three independent experiments is reported, showing the top view of a Z-projection and orthogonal XY and XZ views, along with single-channel images of bacteria (sGFP, green channel) and F-actin (Phalloidin, red channel). Nuclei were stained with TO-PRO (blue). (D) LDH release was measured from 50 µL of basolateral media of infected ALI cultures with PA14 or Δ*sirB2* strains. As control, LDH release was measured from ALI cultures incubated with PBS-free bacteria (CTR). Results from at least five independent experiments are reported with sd. ****, $p < 0.0001$; **, $p < 0.01$ (ANOVA and Tukey's hypothesis test for multiple comparisons). (E) Transepithelial electrical resistance (TEER) of ALI cell layers calculated as the ratio between TEER at 14 h post-infection (hpi) and TEER at 0 hpi and expressed as a percentage (%) for the CTR, PA14, and Δ*sirB2* strains. Results from at least three independent experiments are reported with sd. ****, $p < 0.01$ (ANOVA and Tukey's hypothesis test for multiple comparisons). (F) Colony forming units (CFU/mL) of PA14 and Δ*sirB2* strains in the apical (left graph) or basolateral (right graph) chambers of the transwells. Results from at least five independent experiments are reported with sd. **, $p < 0.01$ (ANOVA and Tukey's hypothesis test for multiple comparisons).

increased lethality of Δ*sirB2* strain might be linked with the heightened production of virulence determinants.

To confirm the results observed in *G. mellonella*, we tested the effects of *sirB2* deletion in an infection model based on fully differentiated human airway epithelial cell cultures at the air-liquid interface (ALI cultures). Confocal microscopy analysis of infected cultures showed that inactivation of the *sirB2* gene (Figure 2C) led to the formation of large cellular aggregates on top of the apical layer scattered through different areas of the cell cultures, compatible with induction of biofilm formation in the mutant (Figure 2C). Furthermore, microscopy observations indicated that the epithelium was more damaged in the cultures infected with the wild-type PA14 strain (Figure 2C). Consistent with this observation, LDH release, which directly correlates with the level of epithelial damage, was higher in response to the wild-type strain than to the Δ*sirB2* mutant (Figure 2D). Yet, the overall discontinuity of the epithelial monolayer was similar between the wild-type and the Δ*sirB2* strain, as indicated by the transepithelial electrical resistance (TEER) of the cell cultures (Figure 2E). However, Δ*sirB2* exhibited slightly higher, though not statistically significant, residual TEER (WT: 5%; Δ*sirB2*: 16%). In addition, while the total number of bacteria colonizing the apical section of the ALI cultures was similar between the wild type and the Δ*sirB2* mutant (Figure 2F), we observed that the Δ*sirB2* mutant strain was more proficient in crossing the epithelial cell layer, resulting in a significantly higher bacterial titer in the basolateral compartments of the ALI cultures (Figure 2F).

Deletion of the sirB2 gene stimulates biofilm formation and virulence factor production in vitro

As deletion of the *sirB2* gene led to increased bacterial aggregation in ALI cultures, we investigated biofilm formation *in vitro* by measuring adhesion to a plastic surface and by evaluating pellicle formation at the air-liquid interface (Figure 3A–C). Inactivation of *sirB2* led to a visible increase in biofilm formation in both models (Figure 3A) with a two- to three-fold increase in adhesion (Figure 3B) and resulting in three to six times more pellicle (Figure 3C), confirming the effect of the gene deletion on biofilm formation.

As the second messenger c-di-GMP acts as a key regulator of the sessile lifestyle and orchestrates the expression of several biofilm determinants [62], we investigated whether the phenotypes observed in the Δ*sirB2* strain could be related to a general modulation of c-di-GMP production rather than the induction of specific biofilm components. Using a c-di-GMP-responsive reporter strain based on the transcriptional fusion of the *cdrA* promoter and the *luxCDABE* operon (P*cdrA::luxCDABE*) [63], we observed that the deletion of *sirB2* led to a 2.8-fold increase in P*cdrA::luxCDABE* activity, indicating an increase in c-di-GMP levels in the mutant strain (Figure 3D).

Switching to a biofilm lifestyle is often associated with reduced virulence during infections. Yet, we observed that the Δ*sirB2* mutant was much more lethal in the *G. mellonella* infection model (Figure 2A). Thus, we measured *in vitro* the production of *P. aeruginosa* main virulence factors. Production of pyocyanin, a phenazine with a cytotoxic effect against eukaryotic cells [64], was stimulated ca. 2 times (Figure 3E). Likewise, pyoverdine, the major *P. aeruginosa* siderophore [65], was increased three times in the Δ*sirB2* strain.

Several exoproducts are essential for *P. aeruginosa* pathogenicity. Secreted endopeptidases, such as the proteases LasA and LasB, are particularly relevant. They contribute to the degradation of a wide array of eukaryotic proteins, favoring the penetration of the bacteria and disrupting host physical barriers [6,66,67]. Both secreted protease and elastase activity were strongly enhanced in the Δ*sirB2* mutant (Figure 3E).

Different sirB2 gene mutations lead to increased emergence of rugose small colony variants (RSCVs) due to dysregulation of the wsp system

The evolution of genetically heterogeneous subpopulations represents an essential survival strategy in *P. aeruginosa* long-term infections [24]. Rugose small colony variants (RSCVs) are a typical phenotype observed in *P. aeruginosa* isolates from chronic CF patients. RSCVs display unique phenotypic properties, such as reduced colony size on solid media, increased biofilm formation [19,20,24], and a red phenotype on agar plates supplemented with the amyloid- and polysaccharide-binding dye Congo Red (CR). When isolating static biofilm-growing Δ*sirB2* cultures on LB or CR agar plates, we observed the appearance of small-sized colonies at a high frequency compared to the wild type (Fig. S3A). The same phenotypic diversification was not observed in overnight cultures grown in shaking in LB and SCFM2 medium, indicating a potential effect of the growth lifestyle rather than specific nutritional cues (Fig. S3A).

Plating on CR-supplemented agar media showed that, while the wild type displayed a homogenous population of normally sized white colonies (Figure 4A), inactivation of the *sirB2* gene led to

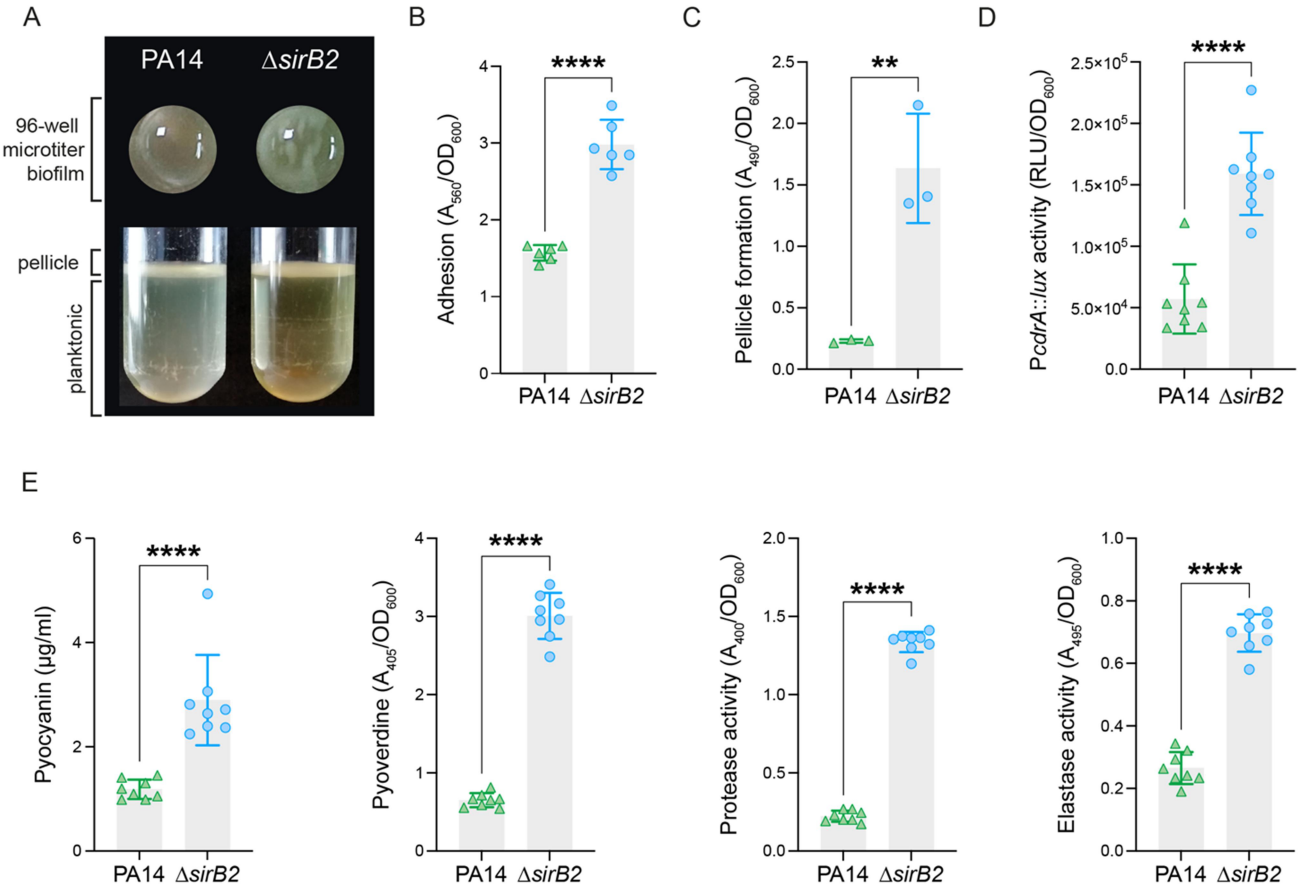

Figure 3. Biofilm and virulence factors production in the *P. aeruginosa* Δ*sirB2* strain. (A) Eepresentative pictures of biofilms formed on 96-well microtiter plates (top) and pellicle formed at the air-liquid phase in a tube (bottom) of *P. aeruginosa* PA14 and Δ*sirB2* strains. (B, C) Effect of the lack of *sirB2* gene on biofilm formation expressed as adhesion units and pellicle formation. PA14 and Δ*sirB2* cultures were grown in static conditions at 37°C in 96-well microtiter plates (B) or 15 mL tubes (C). After 24 hrs of growth, the crystal violet (CV) staining was used to detect the adhesion units grown on the plastic surface, while Congo red (CR) powder was used to detect pellicles formed at the air-liquid interface. Results from at least three independent experiments are reported with sd. ****, $p < 0.0001$ (two-tailed unpaired t-test). (D) Activity of the P*cdrA* promoter, reported as RLU/OD_{600}, in PA14 and Δ*sirB2* cultures grown at 37°C under static conditions for 20 hrs. Results from eight independent experiments are reported with sd. ****, $p < 0.0001$ (two-tailed unpaired t-test). (E) Effect of the lack of *sirB2* gene on the pyocyanin, pyoverdine, proteases, and elastase production measured from the supernatants of PA14 and Δ*sirB2* cultures grown at 37°C in 96-well microtiter plates for 24 h in static conditions. Results from at least three independent experiments are reported with sd. ****, $p < 0.0001$ (two-tailed unpaired t-test).

the appearance of a mixed population made up of white colonies (standard colonies, named as Δ*sirB2*) and red colonies (RSCVs, named as $\Delta sirB2_{RSCV}$). RSCVs represented up to 65% of the population in the Δ*sirB2* mutant and less than 10% in the wild-type strain, both in LB (Figure 4B) and SCFM2 media (Fig. S3B), when cultures were grown in static conditions. At first, we wondered whether RSCVs phenotypes could depend on polar effects or genetic instability induced by the *sirB2* deletion rather than the lack of expression of the gene.

Therefore, we generated different alleles of the *sirB2* gene: we introduced two stop codons at the beginning of the ORF to prevent protein synthesis, maintaining the genetic locus otherwise intact ($sirB2_{mutated}$); we deleted 91 nt in the distal portion of the *sirB2* gene to generate a truncated protein ($sirB2_{truncated}$). Both $sirB2_{mutated}$ and the $sirB2_{truncated}$ strains showed increased adhesion units (Figure 4A) and RSCVs emergence frequencies (Figure 4B), like the deletion mutant Δ*sirB2*. These results strongly suggest that the lack of a functional SirB2 protein, rather than indirect effects due to the gene deletion, was responsible for the phenotypes observed.

The emergence of RSCVs is associated with the acquisition of genetic mutations [19,20,24]. We performed single-colony whole-genome sequencing analysis on PA14 (white colony), Δ*sirB2* (white colony), and $\Delta sirB2_{RSCV}$ (red colony), which identified

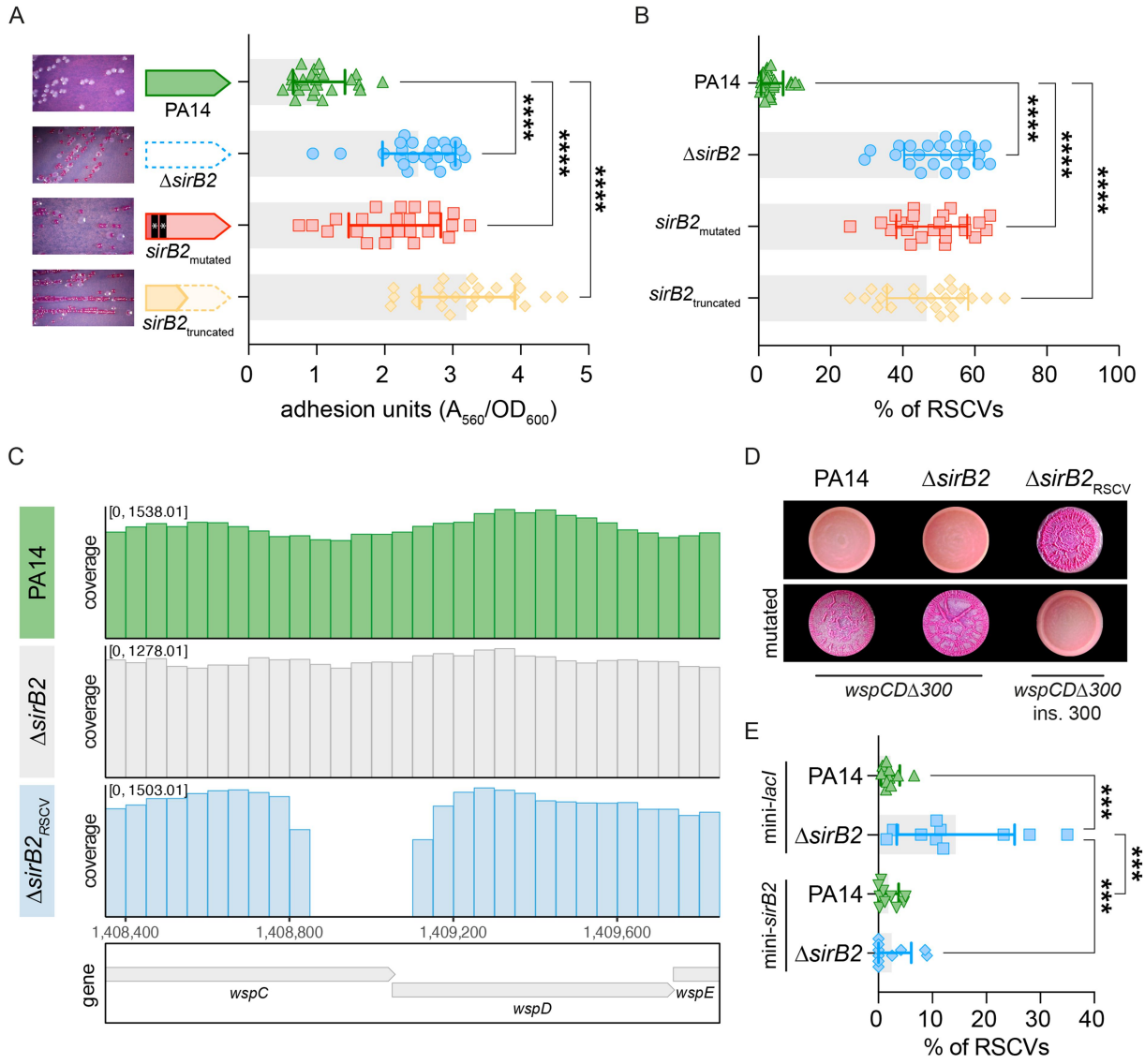

Figure 4. The PA14 Δ*sirB2* genetic background selects for rugose small colony variants (RSCVs). (A) Adhesion to plastic surface of *P. aeruginosa* PA14, Δ*sirB2*, $sirB2_{mutated}$ (two stop-codon mutations), and $sirB2_{truncated}$ (91-nt deletion of the distal portion of the *sirB2*) strains in LB medium after 24 hours incubation in static conditions. Results from 24 independent experiments are reported with sd. ****, $p < 0.0001$ (ANOVA and Tukey's hypothesis test for multiple comparisons). (B) RSCVs percentage in PA14, Δ*sirB2*, $sirB2_{mutated}$ and $sirB2_{truncated}$ populations. The percentage was calculated as the number of the RSCVs (red) divided by the total number of the colonies growing on CR agar plates. Results from 24 independent experiments are reported with sd. ****, $p < 0.0001$ (ANOVA and Tukey's hypothesis test for multiple comparisons). (C) Schematic representation of the *wspCD* genetic locus and its sequencing coverage in the PA14, Δ*sirB2*, and $\Delta sirB2_{RSCV}$ strains. (D) Effect of the deletion of the 318bp region between the *wspC* and *wspD* genes or its reversion to the wild-type sequence on the colony biofilm phenotype of PA14, Δ*sirB2*, and $\Delta sirB2_{RSCV}$ cultures spotted onto CR agar plates. Biofilms were grown at 25°C for at least 72 h before image acquisition, and one representative picture of three independent experiments is shown. (E) Percentage of RSCVs in PA14 and the Δ*sirB2* knockout mutant strains carrying the chromosomally integrated mini-*lacI* plasmid with or without the *sirB2* gene. Results from 10 independent experiments are reported with sd. ****, $p < 0.0001$ (ANOVA and Tukey's hypothesis test for multiple comparisons).

a 318bp-long deletion in the *wsp* genetic locus (from nt 1,408,822 to nt 1,409,140 of the PA14 genome), spanning between the *wspC* and *wspD* genes (Figure 4C), only present in the $\Delta sirB2_{RSCV}$ genome.

When we artificially recreated the deletion through homologous recombination in the PA14 wild-type and Δ*sirB2* strains, we observed a transition from white and large colonies of the parental strains to an RSCVs phenotype on CR-agar plates (Figure 4D). At the same time, restoration of the genetic locus in the $\Delta sirB2_{RSCV}$ strain induced a reversion of the RSCVs phenotype with the appearance of smooth and white colonies, clearly indicating that the deletion is responsible for RSCVs emergence.

We also identified the same 318-bp-long deletion upon sequencing the *wsp* genetic locus in RSCVs obtained from *sirB2*$_{mutated}$ and the *sirB2*$_{truncated}$ strains (Fig. S4), suggesting that acquisition of the mutation depends on the lack of a functional SirB2 protein. In addition, the frequency of the RSCVs emergence dramatically decreased when we ectopically expressed a wild-type copy of the *sirB2* gene in a Δ*sirB2* background using the integrative mini-*lacI* plasmid (Figure 4E). Indeed, the Δ*sirB2* mini-*sirB2* strain showed an RSCVs percentage in the population similar to the wild-type strain harboring either the mini-*sirB2* or the empty vector mini-*lacI*.

The *wspC* and *wspD* genes are part of a regulatory system that controls the activity of the diguanylate cyclase WspR and, in turn, the production of the Pel exopolysaccharide. When we knocked out the *pelB* gene in the Δ*sirB2*$_{RSCV}$ strain, we observed a complete reversion of the RSCVs phenotype (Fig. S5), indicating that the mutation selected in a *ΔsirB2* background is linked to WspR activation and Pel overproduction.

The lack of SirB2 is linked with redox imbalance and defective respiration in anaerobiosis

The emergence of RSCVs has been described as an evolutionary strategy to counteract redox imbalance stemming from suboptimal NADH oxidation caused by restricted access to O_2 as a terminal acceptor in standing cultures [18]. Thus, we evaluated the total amount of nicotinamide adenine dinucleotide in both its oxidized (NAD^+) and reduced (NADH) forms in the wild-type PA14 and mutant Δ*sirB2* strains in static culture during early growth (8 h after inoculation). Single-cell isolation and cell counting on CR agar plates of the tested cultures confirmed the absence of RSCVs in the WT or mutant strains. This indicates that RSCVs emerge later during growth, potentially at higher cell densities when oxygen access is more limited. However, we observed that while NAD^+ concentration remained similar, the reduced form of the dinucleotide was higher in the Δ*sirB2* mutant (Figure 5A). Therefore, inactivation of *sirB2* increased the overall NADH/NAD^+ ratio, which would in turn promote the emergence of RSCVs, as previously noted in standing cultures [18]. Redox imbalance with defective NADH oxidation may be related to issues with electron transfer during respiration. As RSCVs are selected to overcome redox imbalance in populations experiencing O_2 deprivation during static growth [18], we reasoned that the lack of SirB2 protein might result in electron transfer defects in oxygen-depleted conditions. Therefore, we evaluate the growth of wild-type and mutant strains in anaerobiosis, where access to oxygen through RSCV selection cannot be achieved [18]. When grown in LB medium or minimal medium with glucose as a carbon source (M9G) the Δ*sirB2* strain showed a ca. 20% reduction in biomass yield (Figure 5B). The growth defect was aggravated when succinate was used as carbon source instead of glucose (M9S) (Figure 5B): when succinate is used as carbon source, energy production almost solely depends on the electron transport chain (ETC) and on access to the quinone pool through the activity of succinate dehydrogenase. The addition of citrate to the M9S medium (M9S/C) completely abolished Δ*sirB2* growth. Citrate feeds into the TCA cycle before succinate dehydrogenase, contributing to electron transport via complex 2. However, citrate generates additional reduced NADH, which might further aggravate the redox imbalance caused by the deletion of *sirB2* (Figure 5A). Growth defects in anaerobiosis could be rescued by switching to a fermentative, non-respiratory, metabolism with the addition of L-arginine in the absence of NO_3^- (Figure 5B), suggesting that the fitness defect is indeed associated with anaerobic respiration.

As defects in the ubiquinone pool are connected with stable RSCVs appearance [29], and might particularly affect energy metabolism relying strictly on the activity of succinate dehydrogenase, i.e. in M9S, we evaluated whether the addition of ubiquinone 9 (UQ_9), the major ubiquinone supporting *P. aeruginosa* anaerobic respiration [68], could restore the fitness of the Δ*sirB2* strain. As a control, we included a Δ*ubiU* mutant, defective in anaerobic UQ_9 biosynthesis [68], alone or in combination with the *sirB2* deletion. In LB medium, the Δ*ubiU* strains showed a marked growth defect (ca. 60%) (Figure 5C), as expected. Supplementation with 5 µM UQ_9 slightly but significantly improved the growth of both Δ*ubiU* and Δ*sirB2*Δ*ubiU* strains, suggesting a partial functional complementation by the exogenous ubiquinone, which, however, might not completely rescue the phenotype due a limited penetration and assembly in the membrane.

Notably, *sirB2* inactivation in the Δ*ubiU* background did not further exacerbate the growth reduction, and, at the same time, UQ_9 addition failed to restore the *sirB2* phenotype in either LB or M9S media (Figure 5C). These results suggest that *sirB2*-dependent fitness loss is not primarily due to perturbations in UQ_9 biosynthesis. Interestingly, in M9S (Figure 5C), we observed an opposite effect: *sirB2* deletion had a substantial impact on growth, as previously shown (Figure 5B). In contrast, the

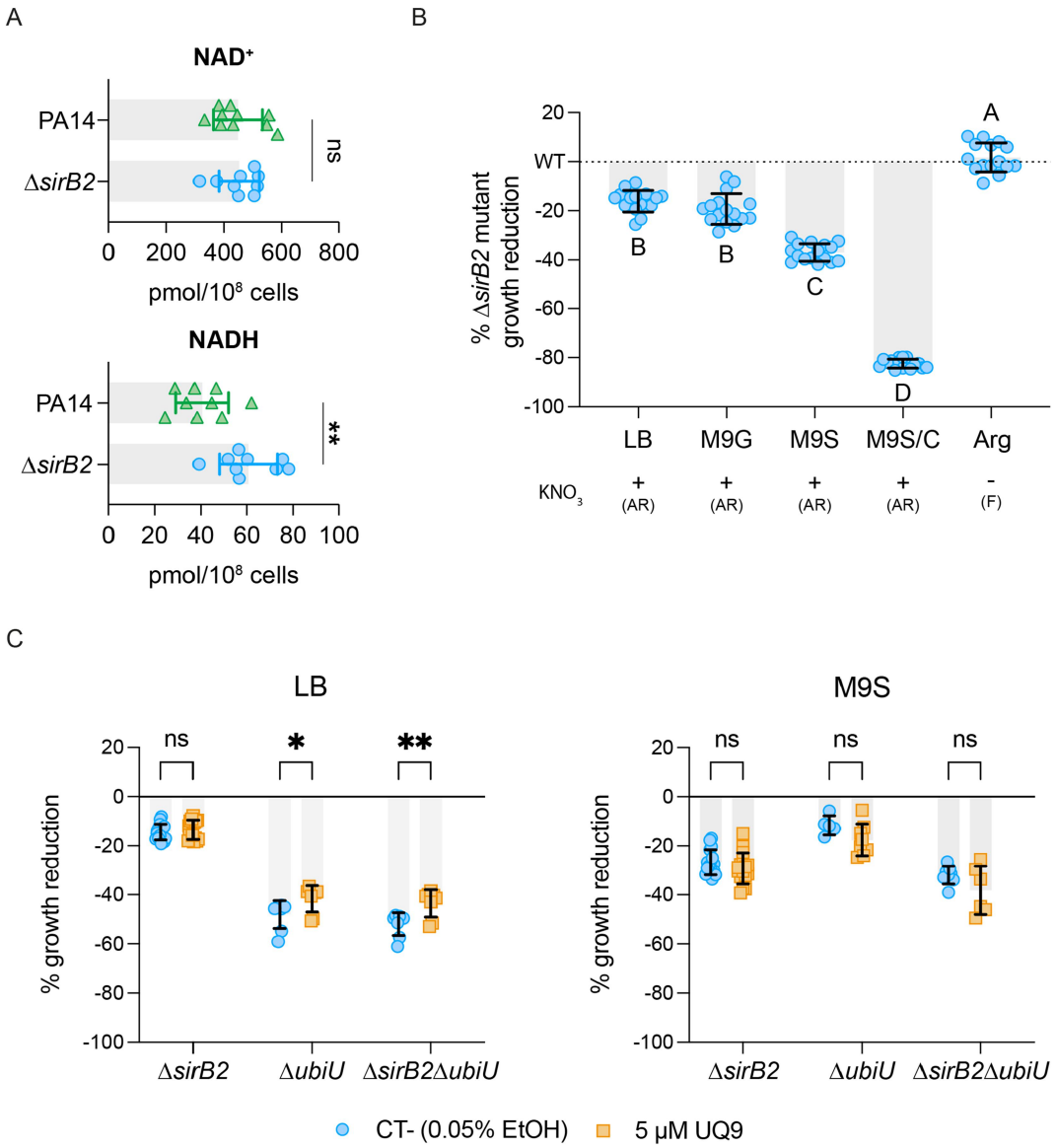

Figure 5. Inactivation of the *sirB2* leads to NADH accumulation and fitness defects during anaerobic respiration. (A) Quantification of NAD^+ and NADH concentration, expressed as pmol/cells from cell pellets of *P. aeruginosa* PA14 and Δ*sirB2* standing cultures grown in LB for 8 h at 37°C using the NAD/NADH-Glo™ assay protocol (Promega). Results from at least nine independent experiments are reported with sd. **, $p < 0.01$ (two-tailed unpaired t-test). (B) Percentage of growth reduction in the Δ*sirB2* mutant in anaerobic conditions in LB, M9G, M9S, or M9S/C medium using nitrate as an electron acceptor (AR, anaerobic respiration) or grown in LB medium without nitrate using arginine for fermentation (F). The growth is expressed as the percentage of reduction in the Δ*sirB2* bacterial yield compared to the PA14 strain grown in the same conditions. Results from 16 independent experiments are reported with sd. Letters indicate significant within-group differences between treatments (one-way ANOVA with Tukey's test for multiple comparisons). (C) Percentage of growth reduction in the Δ*sirB2* mutant, and UQ_9-defective strains Δ*ubiU* and Δ*sirB2*Δ*ubiU* in anaerobic conditions in LB and M9S media using nitrate as an electron acceptor compared to the PA14 strain. Results from at least six independent experiments are reported with sd. *, $p < 0.05$; **, $p < 0.01$ (two-way ANOVA with šídák's multiple comparisons test).

Δ*ubiU* mutation showed a negligible effect. Yet, deletion of *sirB2* in the Δ*ubiU* genetic background further reduced growth, and UQ_9 failed to rescue it. Overall, these observations suggest that *ubiU* is not essential under the tested condition and that SirB2 acts independently of UQ_9 biosynthesis, possibly affecting growth in anaerobiosis via different mechanisms.

Discussion

P. aeruginosa CF infections are challenging to eradicate, and progressive tissue degradation associated with repeated infectious relapses leads to morbidity and, eventually, death [2]. In CF lungs, *P. aeruginosa* infection typically progresses clonally from a single environmentally acquired strain, which, throughout long-

term infections, undergoes extensive genetic and phenotypic adaptations that increase its fitness in the lung environment [2,16,24].

Despite high genetic diversity, lung-adapted *P. aeruginosa* populations share a common transcriptional program in CF lungs stemming from the complex integration of long-term genetic adaptation and response to the unique host conditions. A large fraction of the genes is differentially expressed *in vivo* compared to standard laboratory conditions [2,16,30,31]. More than 50% of genes stimulated *in vivo* are either of unknown function or poorly characterized, highlighting how several processes involved in *P. aeruginosa*-host interaction are still elusive.

In this work, we focused on the gene of unknown function *sirB2* (PA14_RS04555), whose expression is stimulated in clinical isolates growing in CF airways [32] and shares a high degree of homology with the *Salmonella enterica* serovar Typhimurium *sirB2* gene, which was described to impact the pathogen invasiveness [55,56].

We observed that inactivation of *sirB2* increased lethality in an invertebrate infection model. Consistent with this result, the Δ*sirB2* strain produced more virulence factors such as pyocyanin, pyoverdine, elastase, and proteases than its parental strain (Figure 3). Secreted virulence factors are associated with the degradation of extraepithelial components of the respiratory barriers, promoting tissue damage and favoring dissemination in the host [67,69,70]. For example, LasB elastase degrades elastin and collagen and disrupts tight junctions, fostering tissue invasion [66,71]. We observed that many bacteria crossed the epithelial layer when we evaluated the infection process of the Δ*sirB2* strain in the epithelial airway culture infection model (Figure 2E). Still, the epithelial integrity was compromised to the same extent in both the wild-type and the Δ*sirB2* strains, with the latter showing a slightly higher TEER level. Transmigration to the basolateral layer is a complex process that requires type 4 pili, the type 3 secretion system (T3SS), and flagellar motility [72]. In addition, the type 6 secretion system (T6SS) promotes the preferential invasion of goblet cells and epithelial barrier breaching from within [73]. T6SS is co-stimulated with biofilm formation by high concentrations of second messenger c-di-GMP [74,75], a condition that characterizes the Δ*sirB2* mutant. In this scenario, and possibly in combination with other features such as biofilm growth, the mutant strain would cross the epithelium better than the wild type, increasing the number of cells at the basolateral level without, however, causing much damage to the epithelium itself despite the increased production of virulence factors (Figure 3). Indeed, in ALI model, LDH release from epithelial cells, indicating a cytotoxic effect by bacteria, was slightly lower for the Δ*sirB2* mutant (Figure 2). However, an increase in *ΔsirB2* transmigration could lead to a systemic diffusion of the pathogen, and, together with a potential heightened immune response, which is missing from the ALI model, could explain the increased lethality in the *G. mellonella* model.

The regulation of the *sirB2* gene appears to be complex. Just by sequence prediction, we could identify the AmrZ protein and the cAMP-Vfr complex as *sirB2* repressors. AmrZ activates the expression of biofilm determinants, such as the exopolysaccharides alginate and Pel, and the CdrA diguanylate cyclase, while repressing acute virulence factors, including flagella [59,60,76]. AmrZ activity is positively regulated by membrane stress through the alternative sigma factor AlgU/AlgT [77,78]. As SirB2 is a predicted membrane protein, repression of the *sirB2* gene by AmrZ might be mediated by membrane perturbation. The cAMP-Vfr complex acts as a global regulator of virulence factor expression in *P. aeruginosa*; thus, repression by cAMP-Vfr would be consistent with *sirB2* being a negative effector on virulence, albeit indirectly (Figure 3). Interestingly, induction of the AlgU regulon inhibits cAMP-Vfr signaling [79] but induces AmrZ, another negative regulator for *sirB2*. Thus, SirB2 would be generally expressed and exert its activity in conditions where the cAMP-Vfr regulon is inactive, namely, as a result of common direct (*vfr*) [80] mutations, or in conditions leading to an increase in intracellular concentrations of the second messenger c-di-GMP, such as during biofilm formation [81]. Both conditions have been described in clinical isolates from CF patients [16]. We also observed a dependence of *sirB2* expression on growth phase and conditions, specifically at the late exponential phase or in static conditions, *i.e.*, when either nutrients or oxygen availability are limited, further strengthening the link with the host environment.

Although not in absolute terms, it is well established that the production of acute virulence determinants is reduced when *P. aeruginosa* transitions to a sessile lifestyle by forming cellular aggregates or more extensive biofilms, typical traits selected during long-term infections [16,30]. The *sirB2* mutant displayed both phenotypes together. Proteases, elastases, and pyocyanin production are controlled by quorum sensing (QS) [3,6,10], which is activated at high cell densities, such as those in adherent communities, explaining the divergent phenotypes observed in the Δ*sirB2* strain. The co-occurrence of acute virulence determinants and biofilm formation was also observed in several clinical isolates showing genetically heterogeneous populations

characterized by the emergence of the rugose small-colony variant phenotype (RSCVs) [28,82–84]. Our data suggest that lacking a functional *sirB2* gene induces RSCVs emergence at a frequency 40 to 60 times higher than the PA14 wild-type strain. This effect occurs only when the mutant is grown in static conditions at high cell densities after at least 8 hours of growth, *i.e.*, when *sirB2* expression is higher in our experimental setup. Despite the type of mutations introduced in the *sirB2* locus, our results indicated that the emergence of RSCVs depended on a specific 318-bp-long deletion in the *wsp* locus. Deregulation of the *wsp* locus is one of the most frequent genetic mutations leading to RSCVs phenotype [19,20,24,28] and is associated with uncontrolled activation of the WspR diguanylate cyclase. A constitutively activated WpsR leads to increased c-di-GMP concentrations and hyperproduction of the Pel polysaccharide, an essential component of biofilm matrix and potential target of anti-biofilm strategies [85]. Both conditions indeed characterize the RSCVs appearing in Δ*sirB2* population.

These observations have important implications: *sirB2* is not directly involved in controlling virulence and biofilm formation, and its higher expression in vivo would not reasonably lead to their inhibition; however, the lack of its activity in specific conditions might lead to physiological changes that favor the emergence of RSCVs, potentially as a compensatory effect.

Indeed, several studies have shown that RSCVs emerge in conditions of redox imbalance and hypoxia, such as those found *in vivo* at close contact with the epithelium [86,87] or within biofilms [18,28,29]. In this context, the balance can be restored, for example, using phenazines as alternative electron acceptors [18]. Interestingly, we observed that pyocyanin concentrations increased in the Δ*sirB2* mutant, which might point to an attempt to counteract a redox imbalance in static cultures. In agreement, we observed an accumulation of NADH before RSCV appearance, indicating that inactivation of SirB2 protein might result in an increased NADH/NAD^+ ratio and RSCVs selection.

Overall, this suggests that SirB2 higher expression *in vivo* might be related to its involvement in NADH oxidation processes when access to O_2 as an electron acceptor is limited or impossible. Thus, SirB2 would represent a fitness factor in oxygen-limited environments, such as CF airways. In agreement, *sirB2* deletion caused a decrease in cell growth under anaerobic conditions with nitrate as the sole electron acceptor. Genetic data from clinical isolates also support the impact of SirB2 on survival in the CF lungs. Indeed, we identified a high degree of conservation in the *sirB2* sequence, with a strong indication of purifying selection, and no apparent detection of mutations that lead to the loss of SirB2 function. Mutations like those artificially achieved in our study should severely impair *P. aeruginosa* fitness in the host, leading to the swift disappearance of the population harboring the genetic defect. Although RSCVs have been associated with disease exacerbation and reduced lung function [19], the composition of the cohorts from which we derived our data, mostly young patients without reported exacerbations, may also explain the absence of variants that lead to SirB2 inactivation. Therefore, we cannot exclude that loss-of-function mutations could emerge in specific clinical contexts. This observation aligns with the finding that the *sirB2* mutant exhibits exceptional lethality in the *G. mellonella* model, consistent with the emergence of hypervirulent RSCV populations during larval infection. However, the conditions obtained within the invertebrate model are difficult to translate to the complexity of the human lung environment, where the effects of losing *sirB2* might be more pronounced, and hypervirulence might lead to the extinction of the population, rather than to an evolutionary advantage.

In addition, we observed that the Δ*sirB2* mutation led to reduced fitness in anoxic conditions, when succinate, or succinate and citrate, were used as the sole carbon source. Growth on succinate requires succinate dehydrogenase, a key enzyme in the respiratory chain whose activity heavily relies on the ubiquinone pool. Viability, however, was not affected when energy metabolism was supported by L-arginine fermentation, indicating that the loss of fitness was linked to the anaerobic respiratory chain. Interestingly, the SirB2 homolog of *E. coli*, the YchQ protein, was recently proposed as a potential lipid transporter based on an *in silico* screening [88]. In the same study, two ubiquinol-binding proteins were identified, potentially due to similarities between ubiquinol and polar lipid [88]. Furthermore, strains affected in the production of ubiquinone, and thus the respiratory chain, tend to select for RSCV. However, we could not directly link SirB2 to UQ_9 biosynthesis (Figure 5C). In fact, ubiquinone addition could partially restore the growth defect of strains impaired in O_2-independent UQ9 biosynthesis but not in the *ΔsirB2* mutant, suggesting an involvement of *sirB2* in a yet to be identified ubiquinone-independent pathway.

Similarly, how the redox imbalance caused by *sirB2* inactivation leads to the specific appearance of a 318-bp mutation in the *wsp* operon remains unclear. While the reduced fitness of the Δ*sirB2* mutant clearly represents a strong selective pressure favoring the parallel evolution of RSCV through mutations also observed in other *Pseudomonas* species [89], we could not exclude that

the acquisition of the deletion in the *wsp* locus is only linked to redox imbalance. Indeed, as NADH increase is associated with ROS accumulation and DNA damage [90], specific pathways or stress responses may be directly involved in the process.

Our study shows that the *sirB2* gene is involved in processes that can impact NADH oxidation when oxygen availability is reduced or absent [32], making the gene a genuine fitness factor for *in vivo* growth. This underlines the complexity of anaerobic metabolism and of its interplay with virulence factor production. If validated in more complex animal models, our observations would also suggest that targeting processes that affect the cellular energetic state in anaerobiosis may represent an interesting strategy for controlling *P. aeruginosa* infections.

Acknowledgements

We thank Giordano Rampioni for the kind gift of the mini-CTX1, mini-CTX:*lux*, and pMS402-P*cdrA::lux* plasmids.

Author contributions

CRediT: **Valerio Baldelli:** Conceptualization, Formal analysis, Investigation, Visualization, Writing – original draft; **Stacy Julisa Carrasco Aliaga:** Formal analysis, Investigation, Writing – review & editing; **Claudia Antonella Colque:** Investigation, Visualization; **Francesca Mazzola:** Investigation, Methodology; **Srikanth Ravishankar:** Investigation; **Helle Krogh Johansen:** Resources, Writing – review & editing; **Søren Molin:** Resources, Writing – review & editing; **Nadia Raffaelli:** Methodology, Supervision, Writing – review & editing; **Moira Paroni:** Supervision, Writing – review & editing; **Paolo Landini:** Supervision, Writing – review & editing; **Elio Rossi:** Conceptualization, Data curation, Formal analysis, Funding acquisition, Resources, Supervision, Visualization, Writing – original draft, Writing – review & editing.

Funding

This work was supported by Fondazione Cariplo [2020–3581]. Helle Krogh Johansen was funded by a Challenge grant from Novo Nordisk Fonden [NNF19OC0056411] and The John and Birthe Meyer Foundation.

Disclosure statement

No potential conflict of interest was reported by the author(s).

Data availability statement

The data that support the findings of this study are openly available in Zenodo at https://doi.org/10.5281/zenodo.17628415[57], reference 17,583,704. The raw sequence read data that support the findings of this study are openly available in EMBL-EBI European Nucleotide Archive (ENA) at https://www.ebi.ac.uk/ena/browser/view/PRJEB71096, reference PRJEB71096.

ORCID

Valerio Baldelli http://orcid.org/0000-0001-6698-7061
Stacy Julisa Carrasco Aliaga http://orcid.org/0009-0007-3551-633X
Claudia Antonella Colque http://orcid.org/0000-0003-1782-3145
Francesca Mazzola http://orcid.org/0000-0001-9140-012X
Srikanth Ravishankar http://orcid.org/0000-0002-4904-2303
Helle Krogh Johansen http://orcid.org/0000-0003-0268-3717
Søren Molin http://orcid.org/0000-0002-7973-2639
Nadia Raffaelli http://orcid.org/0000-0002-4458-1789
Moira Paroni http://orcid.org/0000-0001-8199-3128
Paolo Landini http://orcid.org/0000-0003-0999-426X
Elio Rossi http://orcid.org/0000-0002-2042-608X

References

[1] Crone S, Vives-Flórez M, Kvich L, et al. The environmental occurrence of *Pseudomonas aeruginosa*. APMIS Acta Pathol Microbiol Immunol Scand. 2020;128 (3):220–231. doi: 10.1111/apm.13010
[2] Rossi E, La Rosa R, Bartell JA, et al. *Pseudomonas aeruginosa* adaptation and evolution in patients with cystic fibrosis. Nat Rev Microbiol. 2021;19(5):331–342. doi: 10.1038/s41579-020-00477-5
[3] Letizia M, Diggle SP, Whiteley M. *Pseudomonas aeruginosa*: ecology, evolution, pathogenesis and antimicrobial susceptibility. Nat Rev Microbiol. 2025;23 (11):701–717. Available from: https://www.nature.com/articles/s41579-025-01193-8
[4] Moradali MF, Ghods S, Rehm BHA. *Pseudomonas aeruginosa* lifestyle: a paradigm for adaptation, survival, and persistence. Front Cell Infect Microbiol. 2017;7. doi: 10.3389/fcimb.2017.00039
[5] Sadikot RT, Blackwell TS, Christman JW, et al. Pathogen–host interactions in *Pseudomonas aeruginosa* pneumonia. Am J Respir Crit Care Med. 2005;171 (11):1209–1223. doi: 10.1164/rccm.200408-1044SO
[6] Smith RS, Iglewski BHP. *P. aeruginosa* quorum-sensing systems and virulence. Curr Opin Microbiol. 2003;6 (1):56–60. doi: 10.1016/S1369-5274(03)00008-0
[7] Deretic V, Schurr MJ, Yu H. *Pseudomonas aeruginosa*, mucoidy and the chronic infection phenotype in cystic fibrosis. Trends Microbiol. 1995;3(9):351–356. doi: 10.1016/S0966-842X(00)88974-X
[8] Bjarnsholt T, Alhede M, Alhede M, et al. The in vivo biofilm. Trends Microbiol. 2013;21(9):466–474. doi: 10.1016/j.tim.2013.06.002
[9] Wolfgang MC, Lee VT, Gilmore ME, et al. Coordinate regulation of bacterial virulence genes by a novel adenylate cyclase-dependent signaling pathway. Dev Cell. 2003;4(2):253–263. doi: 10.1016/S1534-5807(03)00019-4

[10] Coggan KA, Wolfgang MC. Global regulatory pathways and cross-talk control *Pseudomonas aeruginosa* environmental lifestyle and virulence phenotype. Curr Issues Mol Biol. 2012;14(2):47–70.
[11] West SE, Sample AK, Runyen-Janecky LJ. The Vfr gene product, required for *Pseudomonas aeruginosa* exotoxin A and protease production, belongs to the cyclic AMP receptor protein family. J Bacteriol. 1994;176 (24):7532–7542. doi: 10.1128/jb.176.24.7532-7542.1994
[12] Valentini M, Filloux A. Biofilms and cyclic di-GMP (c-di-GMP) signaling: lessons from *Pseudomonas aeruginosa* and other bacteria. J Biol Chem. 2016;291 (24):12547–12555. doi: 10.1074/jbc.R115.711507
[13] Jennings LK, Dreifus JE, Reichhardt C, et al. *Pseudomonas aeruginosa* aggregates in cystic fibrosis sputum produce exopolysaccharides that likely impede current therapies. Cell Rep. 2021;34(8):108782. doi: 10.1016/j.celrep.2021.108782
[14] Jennings LK, Storek KM, Ledvina HE, et al. Pel is a cationic exopolysaccharide that cross-links extracellular DNA in the *Pseudomonas aeruginosa* biofilm matrix. Proc Natl Acad Sci U S A. 2015;112 (36):11353–11358. doi: 10.1073/pnas.1503058112
[15] Cramer N, Klockgether J, Tümmler B. Microevolution of *Pseudomonas aeruginosa* in the airways of people with cystic fibrosis. Curr Opin Immunol. 2023;83:102328. doi: 10.1016/j.coi.2023.102328
[16] Marvig RL, Sommer LM, Molin S, et al. Convergent evolution and adaptation of *Pseudomonas aeruginosa* within patients with cystic fibrosis. Nat Genet. 2015;47 (1):57–64. doi: 10.1038/ng.3148
[17] Winstanley C, O'Brien S, Brockhurst MA. *Pseudomonas aeruginosa* evolutionary adaptation and diversification in cystic fibrosis chronic lung infections. Trends Microbiol. 2016;24(5):327–337. doi: 10.1016/j.tim.2016.01.008
[18] Besse A, Groleau M-C, Déziel E. Emergence of small colony variants is an adaptive strategy used by *Pseudomonas aeruginosa* to mitigate the effects of redox imbalance. mSphere. 2023;8(2):e0005723. doi: 10.1128/msphere.00057-23
[19] Malone JG. Role of small colony variants in persistence of *Pseudomonas aeruginosa* infections in cystic fibrosis lungs. Infect Drug Resist. 2015;8:237–247. doi: 10.2147/IDR.S68214
[20] Häussler S. Biofilm formation by the small colony variant phenotype of *Pseudomonas aeruginosa*. Environ Microbiol. 2004;6(6):546–551. doi: 10.1111/j.1462-2920.2004.00618.x
[21] Byrd MS, Pang B, Hong W, et al. Direct evaluation of *Pseudomonas aeruginosa* biofilm mediators in a chronic infection model. Infect Immun. 2011;79 (8):3087–3095. doi: 10.1128/IAI.00057-11
[22] Drenkard E, Ausubel FM. *Pseudomonas* biofilm formation and antibiotic resistance are linked to phenotypic variation. Nature. 2002;416(6882): 740–743. doi: 10.1038/416740a
[23] Starkey M, Hickman JH, Ma L, et al. *Pseudomonas aeruginosa* rugose small-colony variants have adaptations that likely promote persistence in the cystic fibrosis lung. J Bacteriol. 2009;191(11):3492–3503. doi: 10.1128/JB.00119-09
[24] Xu A, Zhang X, Wang T, et al. Rugose small colony variant and its hyper-biofilm in *Pseudomonas aeruginosa*: adaption, evolution, and biotechnological potential. Biotechnol Adv. 2021;53:107862. doi: 10.1016/j.biotechadv.2021.107862
[25] D'Argenio DA, Calfee MW, Rainey PB, et al. Autolysis and autoaggregation in *Pseudomonas aeruginosa* colony morphology mutants. J Bacteriol. 2002;184 (23):6481–6489. doi: 10.1128/JB.184.23.6481-6489.2002
[26] Hickman JW, Tifrea DF, Harwood CS. A chemosensory system that regulates biofilm formation through modulation of cyclic diguanylate levels. Proc Natl Acad Sci U S A. 2005;102(40):14422–14427. doi: 10.1073/pnas.0507170102
[27] Malone JG, Jaeger T, Spangler C, et al. YfiBNR mediates cyclic di-GMP dependent small colony variant formation and persistence in *Pseudomonas aeruginosa*. PLoS Pathog. 2010;6(3):e1000804. doi: 10.1371/journal.ppat.1000804
[28] Besse A, Groleau M-C, Trottier M, et al. *Pseudomonas aeruginosa* strains from both clinical and environmental origins readily adopt a stable small colony variant (SCV) phenotype resulting from single mutations in c-di-GMP pathways. Microbiology. 2022. doi: 10.1101/2022.06.02.494627
[29] Pitton M, Oberhaensli S, Appiah F, et al. Mutation to *ispA* produces stable small-colony variants of *Pseudomonas aeruginosa* that have enhanced aminoglycoside resistance. Antimicrob Agents Chemother. 2022;66(7):e0062122. doi: 10.1128/aac.00621-22
[30] Cornforth DM, Dees JL, Ibberson CB, et al. *Pseudomonas aeruginosa* transcriptome during human infection. Proc Natl Acad Sci USA. 2018;115(22): E5125–34. doi: 10.1073/pnas.1717525115
[31] Kordes A, Preusse M, Willger SD, et al. Genetically diverse *Pseudomonas aeruginosa* populations display similar transcriptomic profiles in a cystic fibrosis explanted lung. Nat Commun. 2019;10(1):3397. doi: 10.1038/s41467-019-11414-3
[32] Rossi E, Falcone M, Molin S, et al. High-resolution in situ transcriptomics of *Pseudomonas aeruginosa* unveils genotype independent patho-phenotypes in cystic fibrosis lungs. Nat Commun. 2018;9(1):3459. doi: 10.1038/s41467-018-05944-5
[33] Cao P, Fleming D, Moustafa DA, et al. A *Pseudomonas aeruginosa* small RNA regulates chronic and acute infection. Nature. 2023;618(7964):358–364. doi: 10.1038/s41586-023-06111-7
[34] Frimodt-Møller J, Rossi E, Haagensen JAJ, et al. Mutations causing low level antibiotic resistance ensure bacterial survival in antibiotic-treated hosts. Sci Rep. 2018;8(1):12512. doi: 10.1038/s41598-018-30972-y
[35] Hmelo LR, Borlee BR, Almblad H, et al. Precision-engineering the *Pseudomonas aeruginosa* genome with two-step allelic exchange. Nat Protoc. 2015;10 (11):1820–1841. doi: 10.1038/nprot.2015.115
[36] Genee HJ, Bonde MT, Bagger FO, et al. Software-supported user cloning strategies for site-directed mutagenesis and DNA assembly. ACS Synth Biol. 2015;4(3):342–349. doi: 10.1021/sb500194z
[37] Turner KH, Wessel AK, Palmer GC, et al. Essential genome of *Pseudomonas aeruginosa* in cystic fibrosis

sputum. Proc Natl Acad Sci. 2015;112(13):4110–4115. doi: 10.1073/pnas.1419677112
[38] Choi K-H, Schweizer HP. Mini-Tn7 insertion in bacteria with secondary, non-glmS-linked attTn7 sites: example *Proteus mirabilis* HI4320. Nat Protoc. 2006;1(1):170–178. doi: 10.1038/nprot.2006.26
[39] Coppens L, Lavigne R. Sapphire: a neural network based classifier for σ70 promoter prediction in *Pseudomonas*. BMC Bioinf. 2020;21(1):415. doi: 10.1186/s12859-020-03730-z
[40] Dudek C-A, Jahn D. Prodoric: state-of-the-art database of prokaryotic gene regulation. Nucleic Acids Res. 2022;50(D1):D295–302. doi: 10.1093/nar/gkab1110
[41] Rampioni G, Falcone M, Heeb S, et al. Unravelling the genome-wide contributions of specific 2-alkyl-4-quinolones and PqsE to quorum sensing in *Pseudomonas aeruginosa*. PLoS Pathog. 2016;12(11):e1006029. doi: 10.1371/journal.ppat.1006029
[42] Jander G, Rahme LG, Ausubel FM. Positive correlation between virulence of *Pseudomonas aeruginosa* mutants in mice and insects. J Bacteriol. 2000;182(13):3843–3845. doi: 10.1128/JB.182.13.3843-3845.2000
[43] Rampioni G, Pillai CR, Longo F, et al. Effect of efflux pump inhibition on *Pseudomonas aeruginosa* transcriptome and virulence. Sci Rep. 2017;7(1):11392. doi: 10.1038/s41598-017-11892-9
[44] Pedersen BH, Simões FB, Pogrebnyakov I, et al. Metabolic specialization drives reduced pathogenicity in *Pseudomonas aeruginosa* isolates from cystic fibrosis patients. PLoS Biol. 2024;22(8):e3002781. doi: 10.1371/journal.pbio.3002781
[45] Baldelli V, D'Angelo F, Pavoncello V, et al. Identification of FDA-approved antivirulence drugs targeting the *Pseudomonas aeruginosa* quorum sensing effector protein PqsE. Virulence. 2020;11(1):652–668. doi: 10.1080/21505594.2020.1770508
[46] Fernicola S, Paiardini A, Giardina G, et al. In silico discovery and in vitro validation of catechol-containing sulfonohydrazide compounds as potent inhibitors of the diguanylate cyclase PleD. J Bacteriol. 2016;198(1):147–156. doi: 10.1128/JB.00742-15
[47] Merritt JH, Kadouri DE, O'Toole GA. Growing and analyzing static biofilms. Curr Protoc Microbiol. 2005; Chapter 1:Unit 1B.1. 1). doi: 10.1002/9780471729259.mc01b01s00
[48] Friedman L, Kolter R. Genes involved in matrix formation in *Pseudomonas aeruginosa* PA14 biofilms. Mol Microbiol. 2004;51(3):675–690. doi: 10.1046/j.1365-2958.2003.03877.x
[49] D'Angelo F, Baldelli V, Halliday N, et al. Identification of FDA-approved drugs as antivirulence agents targeting the pqs quorum-sensing system of *Pseudomonas aeruginosa*. Antimicrob Agents Chemother. 2018;62(11):e01296–18. doi: 10.1128/AAC.01296-18
[50] Fortuna A, Bähre H, Visca P, et al. The two *Pseudomonas aeruginosa* DksA stringent response proteins are largely interchangeable at the whole transcriptome level and in the control of virulence-related traits. Environ Microbiol. 2021;23(9):5487–5504. doi: 10.1111/1462-2920.15693
[51] Núñez-García LÁ, Feliciano-Guzmán JM, Mireles-Davalos CD, et al. Genomic and phenotypic characterization of *Pseudomonas aeruginosa* isolates from two Mexican cystic fibrosis attention centers. Microbiol Spectr. 2024;12(12):e01100–24. doi: 10.1128/spectrum.01100-24
[52] Spilker T, LiPuma JJ. Draft genome sequences of 63 *Pseudomonas aeruginosa* isolates recovered from cystic fibrosis sputum. Genome Announc. 2016;4(2):e00231–16. doi: 10.1128/genomeA.00231-16
[53] Graeff R, Lee HC. A novel cycling assay for cellular cADP-ribose with nanomolar sensitivity. Biochem J. 2002;361(2):379–384. doi: 10.1042/bj3610379
[54] Zamporlini F, Ruggieri S, Mazzola F, et al. Novel assay for simultaneous measurement of pyridine mononucleotides synthesizing activities allows dissection of the NAD+ biosynthetic machinery in mammalian cells. FEBS J. 2014;281(22):5104–5119. doi: 10.1111/febs.13050
[55] Johnston C, Pegues DA, Hueck CJ, et al. Transcriptional activation of *Salmonella typhimurium* invasion genes by a member of the phosphorylated response-regulator superfamily. Mol Microbiol. 1996;22(4):715–727. doi: 10.1046/j.1365-2958.1996.d01-1719.x
[56] Rakeman JL, Bonifield HR, Miller SI. A HilA-independent pathway to *Salmonella typhimurium* invasion gene transcription. J Bacteriol. 1999;181(10):3096–3104. doi: 10.1128/JB.181.10.3096-3104.1999
[57] Baldelli V, Carrasco Aliaga SJ, Colque CA, et al. The *Pseudomonas aeruginosa* sirB2 gene is a fitness determinant of anaerobic growth and its inactivation affects virulence and rugose small colony variants emergence. 2025; Available from: https://zenodo.org/doi/10.5281/zenodo.17628415
[58] Dasgupta N, Ferrell EP, Kanack KJ, et al. The gene encoding the major flagellar regulator of *Pseudomonas aeruginosa*, is sigma70 dependent and is downregulated by Vfr, a homolog of *Escherichia coli* cyclic AMP receptor protein. J Bacteriol. 2002;184(19):5240–5250. doi: 10.1128/JB.184.19.5240-5250.2002
[59] Jones CJ, Ryder CR, Mann EE, et al. AmrZ modulates *Pseudomonas aeruginosa* biofilm architecture by directly repressing transcription of the *psl* operon. J Bacteriol. 2013;195(8):1637–1644. doi: 10.1128/JB.02190-12
[60] Baltrus DA, Dougherty K, Diaz B, et al. Evolutionary plasticity of AmrZ regulation in *Pseudomonas*. mSphere. 2018;3(2):e00132–18. doi: 10.1128/mSphere.00132-18
[61] Tsai C-Y, Loh JMS, Proft T. *Galleria mellonella* infection models for the study of bacterial diseases and for antimicrobial drug testing. Virulence. 2016;7(3):214–229. doi: 10.1080/21505594.2015.1135289
[62] Rossi E, Paroni M, Landini P. Biofilm and motility in response to environmental and host-related signals in Gram negative opportunistic pathogens. J Appl Microbiol. 2018;125(6):1587–1602. doi: 10.1111/jam.14089
[63] Pawar SV, Messina M, Rinaldo S, et al. Novel genetic tools to tackle c-di-GMP-dependent signalling in *Pseudomonas aeruginosa*. J Appl Microbiol. 2016;120(1):205–217. doi: 10.1111/jam.12984
[64] Hall S, McDermott C, Anoopkumar-Dukie S, et al. Cellular effects of pyocyanin, a secreted virulence

factor of *Pseudomonas aeruginosa*. Toxins (basel). 2016;8(8):236. doi: 10.3390/toxins8080236

[65] Imperi F, Tiburzi F, Visca P. Molecular basis of pyoverdine siderophore recycling in *Pseudomonas aeruginosa*. Proc Natl Acad Sci U S A. 2009;106 (48):20440–20445. doi: 10.1073/pnas.0908760106

[66] Azghani AO. *Pseudomonas aeruginosa* and epithelial permeability: role of virulence factors elastase and exotoxin A. Am J Respir Cell Mol Biol. 1996;15 (1):132–140. doi: 10.1165/ajrcmb.15.1.8679217

[67] Galloway DR. *Pseudomonas aeruginosa* elastase and elastolysis revisited: recent developments. Mol Microbiol. 1991;5(10):2315–2321. doi: 10.1111/j.1365-2958.1991.tb02076.x

[68] C-D-T V, Michaud J, Elsen S, et al. The O2-independent pathway of ubiquinone biosynthesis is essential for denitrification in *Pseudomonas aeruginosa*. J Biol Chem. 2020;295(27):9021–9032. doi: 10.1074/jbc.RA120.013748

[69] Bucior I, Tran C, Engel J. Assessing *Pseudomonas* virulence using host cells. Methods Mol Biol Clifton NJ. 2014;1149:741–755.

[70] Li X-H, Lee J-H. Quorum sensing-dependent post-secretional activation of extracellular proteases in *Pseudomonas aeruginosa*. J Biol Chem. 2019;294 (51):19635–19644. doi: 10.1074/jbc.RA119.011047

[71] Liu Y-C, Hussain F, Negm O, et al. Contribution of the alkylquinolone quorum-sensing system to the interaction of *Pseudomonas aeruginosa* with bronchial epithelial cells. Front Microbiol. 2018;9:3018. doi: 10.3389/fmicb.2018.03018

[72] Sana TG, Berni B, Bleves S. The T6SSs of *Pseudomonas aeruginosa* strain PAO1 and their effectors: beyond bacterial-cell targeting. Front Cell Infect Microbiol. 2016;6:61. doi: 10.3389/fcimb.2016.00061

[73] Leoni Swart A, Laventie B-J, Sütterlin R, et al. *Pseudomonas aeruginosa* breaches respiratory epithelia through goblet cell invasion in a microtissue model. Nat Microbiol. 2024;9(7):1–13. doi: 10.1038/s41564-024-01718-6

[74] Cheng T, Cheang QW, Xu L, et al. A PilZ domain protein interacts with the transcriptional regulator HinK to regulate type VI secretion system in *Pseudomonas aeruginosa*. J Biol Chem. 2024;300 (3):105741. Available from: https://www.jbc.org/article/S0021-9258(24)00117-0/abstract

[75] Moscoso JA, Mikkelsen H, Heeb S, et al. The *Pseudomonas aeruginosa* sensor RetS switches type III and type VI secretion via c-di-GMP signalling. Environ Microbiol. 2011;13(12):3128–3138. doi: 10.1111/j.1462-2920.2011.02595.x

[76] Hou L, Debru A, Chen Q, et al. AmrZ regulates swarming motility through cyclic di-GMP-dependent motility inhibition and controlling Pel polysaccharide production in *Pseudomonas aeruginosa* PA14. Front Microbiol. 2019;10. doi: 10.3389/fmicb.2019.01847

[77] Baynham PJ, Wozniak DJ. Identification and characterization of AlgZ, an AlgT-dependent DNA-binding protein required for *Pseudomonas aeruginosa algD* transcription. Mol Microbiol. 1996;22(1):97–108. doi: 10.1111/j.1365-2958.1996.tb02659.x

[78] Wozniak DJ, Sprinkle AB, Baynham PJ. Control of *Pseudomonas aeruginosa algZ* expression by the alternative sigma factor AlgT. J Bacteriol. 2003;185 (24):7297–7300. doi: 10.1128/JB.185.24.7297-7300.2003

[79] Jones AK, Fulcher NB, Balzer GJ, et al. Activation of the *Pseudomonas aeruginosa* AlgU regulon through *mucA* mutation inhibits cyclic AMP/Vfr signaling. J Bacteriol. 2010;192(21):5709–5717. doi: 10.1128/JB.00526-10

[80] Mena A, Smith EE, Burns JL, et al. Genetic adaptation of *Pseudomonas aeruginosa* to the airways of cystic fibrosis patients is catalyzed by hypermutation. J Bacteriol. 2008;190(24):7910–7917. doi: 10.1128/JB.01147-08

[81] Almblad H, Harrison JJ, Rybtke M, et al. The cyclic AMP-Vfr signaling pathway in Pseudomonas aeruginosa is inhibited by cyclic di-GMP. J Bacteriol. 2015;197(13):2190–2200. doi: 10.1128/JB.00193-15

[82] Malone JG, Jaeger T, Manfredi P, et al. The YfiBNR signal transduction mechanism reveals novel targets for the evolution of persistent *Pseudomonas aeruginosa* in cystic fibrosis airways. PLoS Pathog. 2012;8(6): e1002760. doi: 10.1371/journal.ppat.1002760

[83] Sabra W, Haddad AM, Zeng A-P. Comparative physiological study of the wild type and the small colony variant of *Pseudomonas aeruginosa* 20265 under controlled growth conditions. World J Microbiol Biotechnol. 2014;30(3):1027–1036. doi: 10.1007/s11274-013-1521-z

[84] von Gotz F, Haussler S, Jordan D, et al. Expression analysis of a highly adherent and cytotoxic small colony variant of *Pseudomonas aeruginosa* isolated from a lung of a patient with cystic fibrosis. J Bacteriol. 2004;186(12):3837–3847. doi: 10.1128/JB.186.12.3837-3847.2004

[85] Datta S, Singh V, Nag S, et al. Marine-derived cytosine arabinoside (ara-C) inhibits biofilm formation by inhibiting PEL operon proteins (Pel A and Pel B) of *Pseudomonas aeruginosa*. An Silico Approach Mol Biotechnol. 2025;67(5):1924–1938. doi: 10.1007/s12033-024-01169-8

[86] Downey DG, Bell SC, Elborn JS. Neutrophils in cystic fibrosis. Thorax. 2009;64(1):81–88. doi: 10.1136/thx.2007.082388

[87] Rada B, Leto TL. Redox warfare between airway epithelial cells and *Pseudomonas*: dual oxidase versus pyocyanin. Immunol Res. 2009;43(1–3):198–209. doi: 10.1007/s12026-008-8071-8

[88] Chou J-C, Decosto CM, Chatterjee P, et al. Rapid proteome-wide prediction of lipid-interacting proteins through ligand-guided structural genomics. 2024. Available from https://www.biorxiv.org/content/10.1101/2024.01.26.577452v1

[89] McDonald MJ, Gehrig SM, Meintjes PL, et al. Adaptive divergence in experimental populations of *Pseudomonas fluorescens*. IV. Genetic constraints guide evolutionary trajectories in a parallel adaptive radiation. Genetics. 2009;183(3):1041–1053. doi: 10.1534/genetics.109.107110

[90] Arce-Rodríguez A, Pankratz D, Preusse M, et al. Dual effect: high NADH levels contribute to efflux-mediated antibiotic resistance but drive lethality mediated by reactive oxygen species. MBio. 2022;13(1):e02434–21. doi: 10.1128/mbio.02434-21